A Multiscale Analysis of the Extreme Weather Events over Western Russia and Northern Pakistan during July 2010

THOMAS J. GALARNEAU JR.*

Cooperative Institute for Research in Environmental Sciences, University of Colorado, Boulder, Colorado

THOMAS M. HAMILL AND RANDALL M. DOLE

NOAA/Earth System Research Laboratory/Physical Sciences Division, Boulder, Colorado

JUDITH PERLWITZ

Cooperative Institute for Research in Environmental Sciences, University of Colorado, Boulder, Colorado

(Manuscript received 25 July 2011, in final form 2 January 2012)

ABSTRACT

This manuscript presents a detailed multiscale analysis—using observations, model analyses, and ensemble forecasts—of the extreme heat wave over Russia and historic floods over Pakistan during late July 2010, with an emphasis on the floods over northern Pakistan. The results show that recirculation of air and dynamically driven subsidence occurring with the intensification of the blocking anticyclone in late July 2010 were key factors for producing the exceptionally warm temperatures over western Russia. Downstream energy dispersion from the blocking region led to trough deepening northwest of Pakistan and ridge building over the Tibetan Plateau, thereby providing the linkage between the Russian heat wave and Pakistan flood events on the large scale, in agreement with previous studies.

The extratropical downstream energy dispersion and enhanced convective outflow on the large scale associated with the active phase of the Madden–Julian oscillation facilitated the formation of an intense upper-level jet northwest of Pakistan. During this same period an intense southeasterly, low-level, barrier jet–like feature formed over northern Pakistan in conjunction with a westward-moving monsoon depression. This low-level jet and deep easterly flow on the equatorward flank of an anomalous anticyclone over the Tibetan Plateau further enhanced the transport of deep tropical moisture into Pakistan and produced a sustained upslope flow and an extended period of active convection, thereby providing an important contribution leading to the exceptional rainfall amounts. The deep easterly flow and intense low-level jet were features that were absent during previous convective episodes over northern Pakistan in 2010, and hence, were likely key factors in the increased severity of the late July event.

1. Introduction

a. Motivation and overview

The summer of 2010 was particularly noteworthy for two high-impact weather events that occurred over eastern Europe and western Asia. Extreme heat, drought, and widespread wildfires occurred over western Russia (Grumm 2011; Barriopedro et al. 2011), while historic rainfall and attendant flooding occurred over northern Pakistan (Houze et al. 2011). Figure 1a illustrates this period of most extreme warmth in the time series of daily maximum and minimum temperatures in Moscow, Russia, for 1 June–31 August 2010. The most extreme temperatures commenced in mid-July and lasted through mid-August as the daily maximum temperature remained above 30°C. These temperatures were the warmest observed and the longest-duration positive anomaly for the period November 2009–October 2010 (Fig. 1b). The time series of area-averaged rainfall over northern Pakistan

* Current affiliation: National Center for Atmospheric Research, Boulder, Colorado.

Corresponding author address: Thomas J. Galarneau Jr., National Center for Atmospheric Research, P.O. Box 3000, Boulder, CO 80307.
E-mail: tomjr@ucar.edu

DOI: 10.1175/MWR-D-11-00191.1

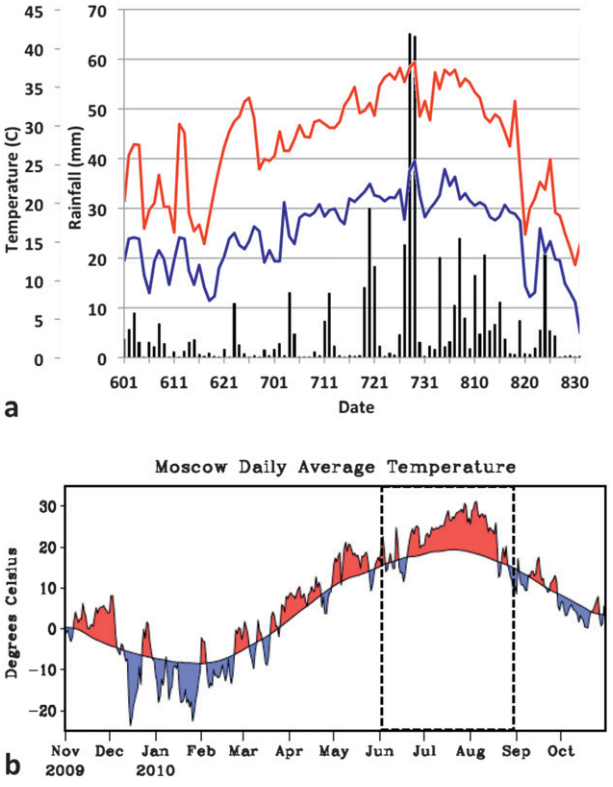

FIG. 1. (a) Time series of daily maximum (red contour) and minimum (blue contour) air temperature at Moscow (station identification 27612), and daily area-average TRMM-derived rainfall over northern Pakistan (black bars) during 1 Jun–31 Aug 2010. The averaging area is indicated by the box annotated in Fig. 2a. (b) Time series of daily average temperature and departure from climatology at Moscow for November 2009–October 2010 [(b) was obtained from Dole et al. (2011, their Fig. 1)].

(the averaging box is indicated in Fig. 2a), derived from the Tropical Rainfall Measuring Mission (TRMM) satellite, shows episodic bursts of heavy rainfall during the summer phase of the Asian monsoon. The wettest period over northern Pakistan occurred from mid-July through late August, in concert with the most intense heat over Moscow (Fig. 1a). Both the Russian heat and the Pakistan rains reached extreme intensities on 28–29 July. The common evolution of the Russian heat and Pakistan rains suggests that these events were dynamically linked (see also Hong et al. 2011; Lau and Kim 2012).

Numerous studies that have rapidly emerged over the last year have considered climatological and predictability aspects of the Russian heat wave and Pakistan flood events. These include large-scale circulation features associated with the Russian heat wave (Dole et al. 2011; Grumm 2011) and the synoptic-scale aspects of the Pakistan floods (e.g., Houze et al. 2011). Houze et al. (2011) also examined the mesoscale precipitation structure of the convective system using TRMM precipitation radar (PR) satellite data. Their results show the only known radar measurements during the period of heavy rainfall and illustrate the widespread stratiform rainfall present during the event. Predictability of the Russian heat wave has been examined for climate and weather time scales (Dole et al. 2011; Matsueda 2011) and for weather time scales for the Pakistan floods (Webster et al. 2011). The large-scale connections between the Russian heat wave and Pakistan floods were examined by Hong et al. (2011) and Lau and Kim (2012). These studies showed how a Rossby wave train extending from the heat wave–producing anticyclone over western Russia connected to the subtropical monsoon region over Southeast Asia. The attendant development of a deep trough over northern Pakistan, northward displacement of the monsoon intraseasonal oscillation, and development of southeasterly low-level flow over northern India (also Houze et al. 2011) all contributed to the heavy rainfall over northern Pakistan.

This aim of this study is fourfold. First, we will examine the connection between the blocking anticyclone over western Russia and the trough–ridge pattern over Pakistan and the Tibetan Plateau. This work complements previous studies by, for example, Lau and Kim (2012) and Hong et al. (2011), but provides a new perspective by conducting an air parcel trajectory analysis to examine the three-dimensional airflow within the blocking anticyclone and the Pakistan flood region, and by considering how downstream amplification and tropical–extratropical interaction affected the behavior and evolution of the upper-level jet and jet-entrance region northwest of Pakistan. Additionally, we will consider the role of the Madden–Julian oscillation (MJO; Madden and Julian 1972) in Tibetan anticyclogenesis and upper-level jet intensification. Second, we will examine the importance of the Tibetan anticyclone in the Pakistan flood event. Houze et al. (2011) discusses how the anticyclone over the Tibetan Plateau played a role in the northwestward advection of deep tropical moisture from the Bay of Bengal region. Our analysis complements the work in Houze et al. (2011), but also addresses how the Tibetan anticyclone was the key factor that was absent in previous lesser-rain events in 2010. Third, we examine the importance of a westward-moving monsoon depression in driving robust southeasterly flow over northern India. Houze et al. (2011) showed this relationship demonstrating that our work is complementary, but we additionally suggest that the southeasterly flow had a barrier jet–like structure and was important in driving intense upslope flow over northern Pakistan, an aspect also missing from previous rain events over northern Pakistan in 2010. Last, we will use ensembles to examine the predictability of the Pakistan

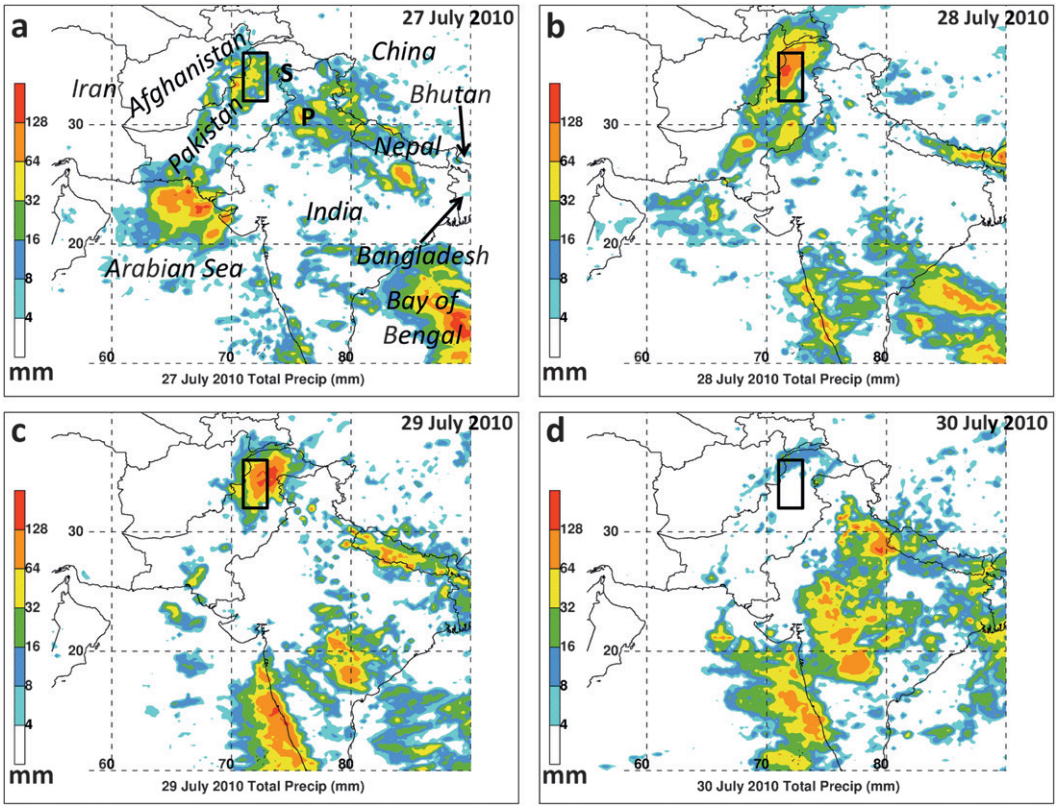

FIG. 2. Daily total TRMM-derived rainfall (shaded according to the color bar in mm) for (a) 27, (b) 28, (c) 29, and (d) 30 Jul 2010. The averaging area for Fig. 1a is annotated as a box in each panel. This box approximately marks the region of heaviest precipitation for the period 27–30 Jul 2010. The Srinigar and Patiala sounding locations are marked S and P, respectively, in (a) and are shown in Fig. 4.

flood event. The ensemble work complements the work by Webster et al. (2011), but additionally uses the ensemble to highlight the key synoptic features that led to heavy rainfall production in the model.

b. Brief background information on extreme heat waves and heavy rainfall

Numerous previous studies have demonstrated a linkage between blocking anticyclones, long-lived extreme heat waves, and drought (e.g., Namias 1982, 1991). For example, major heat waves occurred over the United States in July 1995 (e.g., Changnon et al. 1996; Galarneau et al. 2008), over western Europe in August 2003 (e.g., Burt 2004; Galarneau et al. 2008), and over southeast Australia in February 2004 (Galarneau et al. 2008). All of these heat waves occurred in conjunction with persistent continental anticyclones. Research on these and other cases shows that the extreme nature of some heat waves is maintained both by dynamically driven subsidence and recirculation of air in conjunction with the persistent anticyclone (e.g., Galarneau et al. 2008) and regional land surface feedbacks (e.g., Black et al. 2004; Hao and Bosart 1987; Lyon and Dole 1995; Livezey and Tinker 1996). For the 2010 Russian heat wave, Dole et al. (2011) and Grumm (2011) demonstrated that the above-mentioned mechanisms—dynamical forcing and regional land surface feedbacks—were likely crucial in explaining the event's intensity and persistence, similar to other extreme heat waves over the last century.

The synoptic-scale conditions favorable for heavy rainfall commonly occur along the periphery of blocking anticyclones (e.g., Namias 1936; Weaver and Nigam 2008). Severe mesoscale convective systems have been documented along the poleward periphery of blocking anticyclones over the continental United States in environments with deep instability and strong vertical wind shear (Johns and Hirt 1987). Organized severe convection has also been observed along the equatorward flank of blocking anticyclones over the continental United States and over Australia where mesoscale disturbances in the upper troposphere provide localized regions of enhanced lift, instability, and vertical wind shear (Galarneau and Bosart 2006). In addition to the periphery of anticyclones, heavy rainfall that occurs in

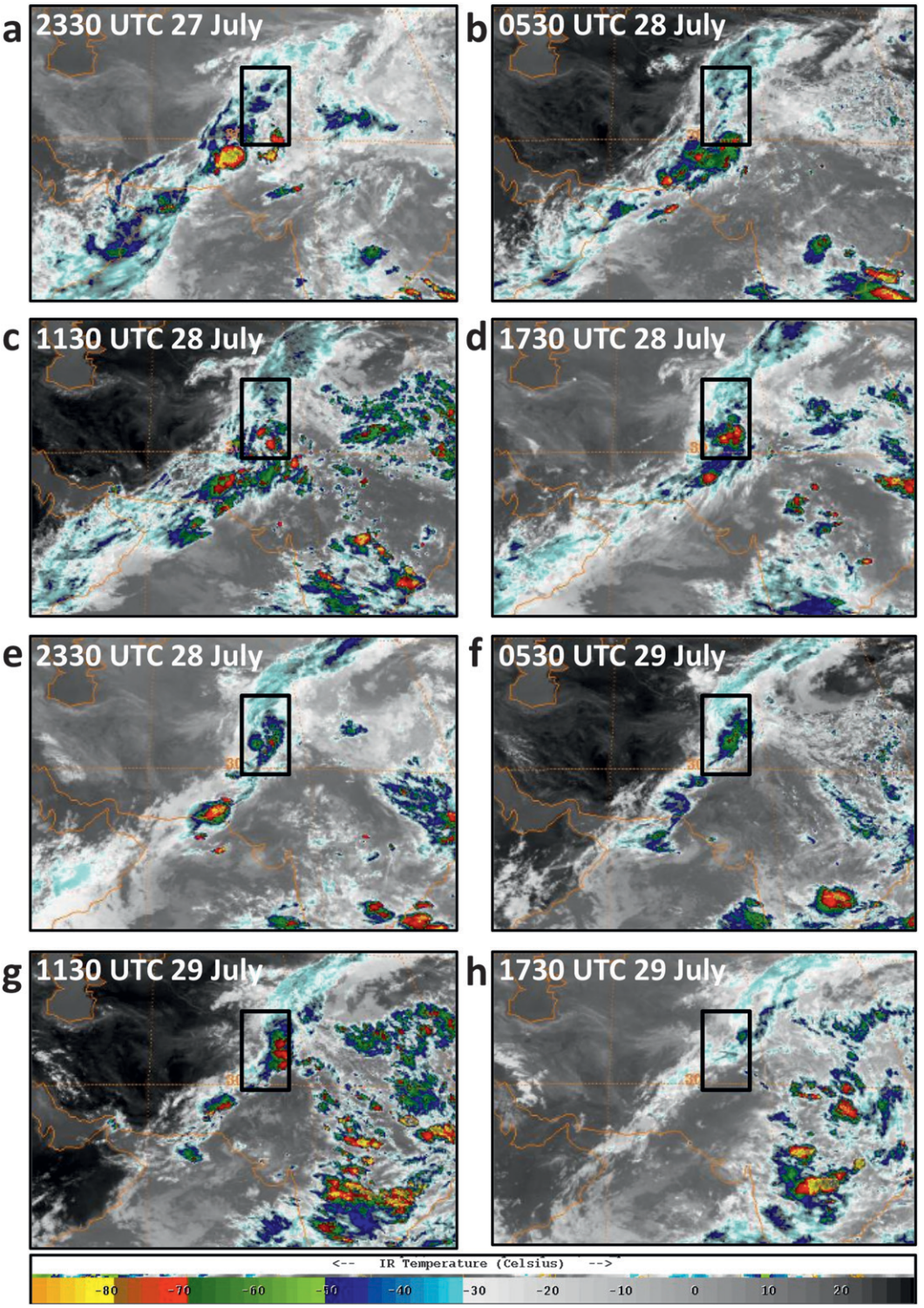

FIG. 3. *Meteosat-7* infrared satellite imagery (shaded according to the color bar in °C) for (a) 2330 UTC 27 Jul, (b) 0530 UTC 28 Jul, (c) 1130 UTC 28 Jul, (d) 1730 UTC 28 Jul, (e) 2330 UTC 28 Jul, (f) 0530 UTC 29 Jul, (g) 1130 UTC 29 Jul, and (h) 1730 UTC 29 Jul 2010. The box annotated in each panel approximately marks the region of heaviest rainfall during 27–30 Jul 2010.

TABLE 1. Listing of the top 10 rainfall totals (mm) and percent of the July monthly climatology from station data over northern Pakistan for 28–30 Jul 2010. Total rainfall and percent of normal for the entire month of July are indicated in parentheses. Data were obtained from the PakMet website (http://www.pakmet.com.pk/).

Station, province	Rainfall (mm)	Percent of July normal
Risalpur, Khyber Pakhtunkhwa	406 (433)	Climatology not available
Islamabad, Punjab	391 (502)	Climatology not available
Cherat, Khyber Pakhtunkhwa	371 (388)	397% (415%)
Murree, Punjab	368 (579)	101% (159%)
Saidu Sharif, Khyber Pakhtunkhwa	334 (471)	219% (309%)
Peshawar AP, Khyber Pakhtunkhwa	333 (402)	722% (872%)
Garhi Dupatta, Azad Kashmir	331 (570)	125% (215%)
Kamra, Punjab	308 (479)	Climatology not available
Rawalakot, Azad Kashmir	295 (521)	Climatology not available
Lower Dir, Khyber Pakhtunkhwa	263 (295)	Climatology not available

seemingly favorable synoptic-scale regimes can be modulated by orography and pose a formidable forecast challenge. Heavy rainfall events associated with orography over the United States (e.g., Maddox et al. 1978; Caracena et al. 1979; Pontrelli et al. 1999; Mo et al. 1995; Pan et al. 2004; Srock and Bosart 2009), European Alps (e.g., Massacand et al. 1998; Rotunno and Ferretti 2001), Taiwan (e.g., Lin et al. 2001, and references therein), and other mountainous regions have all been studied extensively in the literature. Previous work has found that, in general, heavy rainfall near orography occurs in conjunction with a potentially unstable air mass that intersects elevated terrain, abundant low-level moisture, an intense low-level jet, steep orography, and persistent synoptic-scale forcing for ascent.

Orographically influenced rainfall over the monsoonal South Asia region has been studied extensively by Romatschke et al. (2010) and Romatschke and Houze (2011). Heavy rainfall can also occur in rare occasions over the arid mountainous regions of northern Pakistan (Houze et al. 2011). While some of the most intense thunderstorms in the world are observed in this region and along the southwest flank of the Himalayas, they typically do not produce widespread heavy rainfall and flooding because of their limited areal extent and the abundant dry air in the environment associated with westerly flow over the arid terrain to the west (see also Zipser et al. 2006; Houze et al. 2007). Rainfall that occurs in conjunction with the Asian summer monsoon typically occurs farther east over India and northern Bangladesh (Romatschke et al. 2010; Webster et al. 2011), and is modulated on interseasonal time scales by the phase of El Niño–Southern Oscillation (Shukla and Paolina 1983; Kumar et al. 2006) and on intraseasonal time scales by the phase of the MJO (Lawrence and Webster 2001; Webster and Hoyos 2004; Hoyos and Webster 2007). The monsoon convection typically produces much more rainfall compared to the deep convective storms seen farther west over western India and Pakistan. Monsoonal convection over northern Bangladesh occurs in a more moist environment through a deep layer, contributing to larger stratiform rain regions, which can result in heavy rainfall over a broad region (Romatschke and Houze 2011).

c. *Outline*

The remainder of this paper is organized as follows: the datasets and methods used to conduct the case analysis are described in section 2. Section 3 presents a case overview of the Pakistan flood event, while section 4 explores the linkage between the Russian heat wave and Pakistan floods. Section 5 examines the role of tropical–extratropical interaction in upper-level jet intensification. Sections 6 and 7 investigate the physical mechanisms driving the heavy rainfall over Pakistan, while section 8 provides a synthesis of results and concluding remarks.

2. Data and methods

Several datasets were used in the case analysis. Daily surface temperature data for Moscow were obtained

TABLE 2. Listing (from north to south) of 10 climate stations, including (from left to right) their latitude and longitude, 1931–60 July rainfall normal from the World Survey of Climatology (WSC), July rainfall normal from the Pak Met website, and the July 2010 monthly rainfall values. All rainfall values are in mm.

Station	Lat (°N)/lon (°E)	WSC31–60 normal	PakMet normal	2010
Peshawar	34.0°/71.6°	34	46	402
Rawalpindi	33.6°/73.0°	232	305	383
D. I. Khan	31.8°/70.9°	65	61	147
Lahore	31.5°/74.3°	122	218	308
Zhob	31.4°/69.4°	52	61	117
Quetta	30.2°/67.0°	21	16	2
Nokkundi	28.8°/62.7°	1	2	0
Jacobabad	28.3°/68.5°	27	43	132
Jiwani	25.1°/61.8°	9	9	0
Karachi	24.9°/67.1°	101	66	129

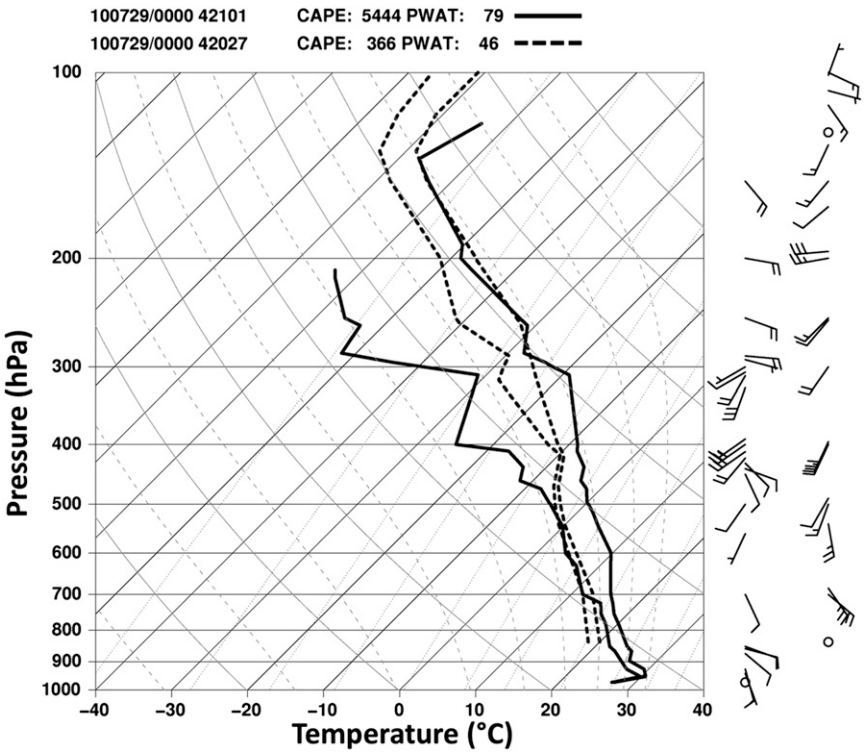

FIG. 4. Skew T–log$p$ diagram of air temperature (°C), dewpoint (°C), and wind (half barb = 2.5 m s^{-1}, full barb = 5.0 m s^{-1}, pennant = 25.0 m s^{-1}) at 0000 UTC 29 Jul 2010 for Patiala (42101; solid line with wind barbs on left) and Srinagar (42027; dashed line with wind barbs on right). CAPE (J kg^{-1}) and total column PW (mm) are labeled at the top of the diagram. Sounding locations are indicated in Fig. 2a.

from the surface data archive available at the National Climatic Data Center (NCDC). Rain gauge data and climatological rainfall information were obtained from the Pakistan Meteorological Department (PakMet; http://www.pakmet.com.pk/). The gridded TRMM_3B42 product (Huffman et al. 2007), available at the National Aeronautics and Space Administration, was used for precipitation analysis. The TRMM-derived precipitation data had 0.25° × 0.25° horizontal resolution at 3-h intervals. Both the *Meteorological Satellite-7* (*Meteosat-7*) geostationary infrared satellite imagery and radiosonde data over Pakistan and India were obtained from NCDC.

Geopotential height mean and anomaly charts and stationary wave activity flux (Plumb 1985) calculations were computed using the 6-hourly National Centers for Environmental Prediction (NCEP)–National Center for Atmospheric Research (NCAR) reanalysis (Kalnay et al. 1996) available at 2.5° × 2.5° resolution. All other analyses and diagnostic calculations were generated using gridded analyses from the NCEP operational gridpoint statistical interpolation (GSI) data assimilation system (Kleist et al. 2011) available at 6-h intervals and at 0.5° × 0.5° horizontal and 50-hPa (25 hPa in the lowest 100 hPa) vertical resolution. Additionally, the NCEP GSI was used at 6-h intervals to compute backward and forward air parcel trajectories, with linear interpolation of the horizontal wind and vertical motion fields at 1-hourly time steps between analysis periods.

Ensemble model analysis of the Pakistan flood event was conducted using the European Centre for Medium-Range Weather Forecasts (ECMWF) ensemble prediction system (EPS). The ECMWF EPS (Buizza et al. 2007) data were obtained from The Observing System Research and Predictability Experiment (THORPEX) Interactive Grand Global Ensemble (TIGGE) archive, consisting of 51 members with a spectral truncation of T639 (corresponding to approximately 32-km horizontal grid spacing) and 62 vertical levels.

3. Case overview

Throughout the summer of 2010, particularly from late June through the end of August, episodic heavy rain events occurred over the mountainous region of northern Pakistan (Fig. 1). Leading up to the heaviest rain event, which occurred on 27–30 July, four heavy rain events

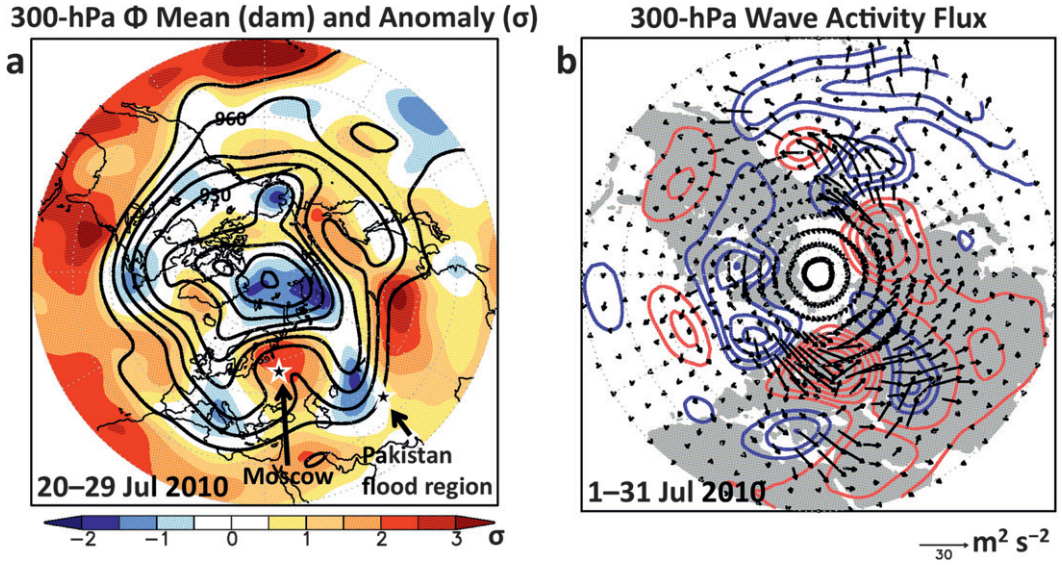

FIG. 5. The 300-hPa (a) geopotential height mean (solid contours every 10 dam) and standardized anomaly (shaded according to the color bar in standard deviation) for 20–29 Jul 2010, and (b) stationary wave activity flux (arrows in $m^2\ s^{-2}$) and streamfunction anomaly (solid contours every $3.0 \times 10^6\ m^2\ s^{-1}$; red contours >0, blue contours <0, zero contour not plotted) from the zonal mean for 1–31 Jul 2010. The anomalies were computed from the long-term (1979–2009) mean. The locations of Moscow and northern Pakistan are marked with stars in (a).

occurred over northern Pakistan on 23 June, 4 July, 12 July, and 19–21 July. It is likely that these precursor rainfall events sufficiently moistened the soils over the rough terrain of northern Pakistan, contributing to increased runoff into the Indus River basin during the 27–30 July event. Maps of the daily TRMM-derived rainfall totals show that rainfall began on 27 July in extreme northeast Afghanistan and northwest Pakistan [Fig. 2a; see also Houze et al. (2011), their Figs. 2g–i, 3]. This rainfall remained over the same region on 28 July and increased in intensity with over 128 mm of rainfall indicated (Fig. 2b). By 29 July, the axis of heaviest rainfall shifted slightly eastward but remained in northern Pakistan and maintained its intensity (Fig. 2c). By 30 July, much of the heaviest rainfall occurred over west-central India while light precipitation occurred over extreme northern Pakistan (Fig. 2d).

Examination of the *Meteosat-7* infrared satellite imagery shows that the most intense convection occurred over southwest Pakistan from late on 27 July through about 0600 UTC 28 July, with evidence of possible widespread stratiform precipitation (as suggested by relatively warm cloud-top temperatures in Fig. 3b; see also Houze et al. 2011) across northern Pakistan by 0600 UTC (Figs. 3a,b). From 1200 UTC 28 July through 1200 UTC 29 July, the most intense convection shifted northward into northern Pakistan and remained nearly stationary over the high terrain (Figs. 3c–g) in the Indus River basin watershed (not shown). During this 24-h period in which the heaviest rains fell (see also Figs. 1, 2b,c), convection continually redeveloped over the mountainous terrain (not shown). This extended period of active convection contributed to the extremely heavy rainfall totals where many stations received well over 200% of their climatological monthly July rainfall in just 48 h (Tables 1, 2).

The soundings from Srinigar and Patiala, India (locations marked in Fig. 2a), at 0000 UTC 29 July illustrate that the extended period of active convection occurred in an extremely moist environment through a deep layer (Fig. 4). The deep-layer veering wind profiles also indicate that the convection occurred in a warm-air advection regime, suggesting that the synoptic-scale environment—marked by likely quasigeostrophic ascent via warm-air advection—was favorable for the development of heavy precipitation. Additionally, the deep tropical moisture, which was highly anomalous for northern Pakistan (see Fig. 4a in Houze et al. 2011), provides an environment capable of increased precipitation efficiency and likely mitigates the development of deep cold pools that can stabilize the environment and allow convection to propagate away from the mountains.

4. Linkage between the Russian heat wave and Pakistan floods

The time-mean 300-hPa geopotential height and anomaly for 20–29 July—the 10-day period leading up

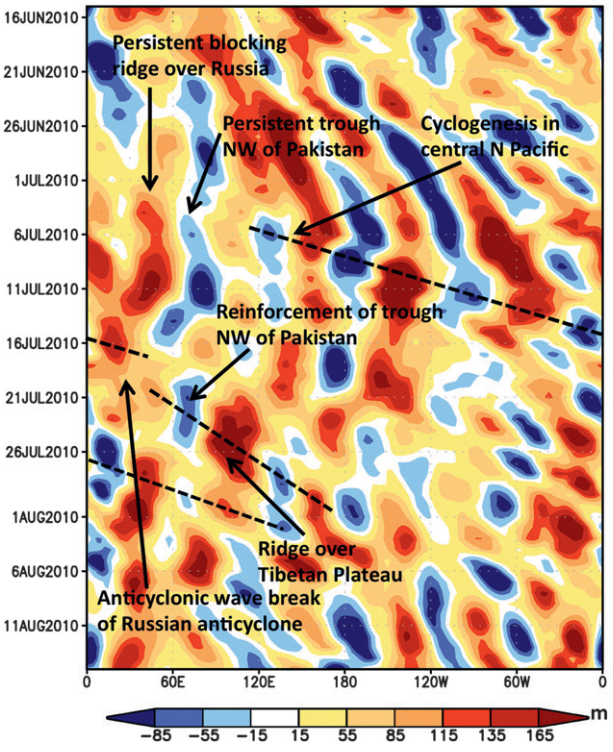

FIG. 6. Time–longitude diagram of 300-hPa geopotential height anomaly (shaded according to the color bar in m) averaged from 35° to 55°N for 15 Jun–15 Aug 2010. The anomalies were computed from the long-term (1979–2009) mean. Key synoptic-scale features and downstream wave packet propagation (dashed lines) are indicated.

to the most extreme heat over western Russian and heaviest rains over northern Pakistan—shows an omega-block pattern extending from western Europe to central Asia (Fig. 5a). The core of the blocking anticyclone was positioned almost directly over Moscow, while flanking troughs were anchored over central Europe and over Asia just northwest of the Pakistan flood region. The configuration of the large-scale pattern reveals that the synoptic-scale weather systems that produced the extreme heat over Russia and rain over Pakistan were both part of the same large-scale omega-block pattern. Stationary wave activity fluxes (Plumb 1985) for July show propagation from an apparent wave source region associated with a trough over the northeastern Atlantic through the blocking anticyclone, and then these fluxes split along two primary branches, one southeastward toward northwest Pakistan and the second eastward across northern Asia (Fig. 5b; see also Hong et al. 2011). There is some indication of southward propagation toward an apparent source over the eastern Mediterranean as well. Possible sources for wave activity over the northeast Atlantic include transient eddy fluxes and diabatic heating. The former is consistent with synoptic-scale eddy straining and wave breaking in the diffluent large-scale flow upstream of the blocking anticyclone, a factor of primary importance for blocking development and maintenance as found in numerous studies (e.g., Schutts 1983). The time–longitude diagram of the 300-hPa geopotential height anomaly for 15 June–15 August shows that both the blocking anticyclone over western Russia (near 35°E) and the downstream flanking trough northwest of Pakistan (near 65°E) were persistent features throughout the summer of 2010 (Fig. 6).

Downstream development began near 150°E on 7 July 2010 in conjunction with extratropical cyclogenesis over the central North Pacific (Fig. 6). The downstream energy propagation led to pattern amplification and anticyclonic wave breaking of the heat wave–producing anticyclone over western Russia during 16–20 July (not shown). The blocking anticyclone quickly became reestablished and downstream amplification contributed to the deepening of the trough near Pakistan by 21 July and intense upper-level anticyclogenesis over the Tibetan Plateau starting on 22 July (Fig. 6). The strengthening of the blocking anticyclone over eastern Europe and western Russia is illustrated by the blocking index formulated originally by Pelly and Hoskins (2003), which defined blocking zones as regions in which the meridional gradient of potential temperature on the dynamic tropopause is positive. Note that the blocking index indicates that blocking was reestablished over eastern Europe and western Russia starting on 26 July (Fig. 7). A second bout of downstream development (along the subtropical jet; not shown) began on 26 July and helped reinforce the amplitude of the trough northwest of Pakistan and ridge over the Tibetan Plateau during 27–30 July (Fig. 6). The importance of pattern amplification in upper-level jet intensification will be examined in the next section.

To examine the linkage between the Russian heat wave and Pakistan floods from a Lagrangian perspective, selected 120-h backward and forward air parcel trajectories were computed at representative times beginning at 1440, 3000, and 5000 m above mean sea level (MSL) near Moscow and over northern Pakistan (Fig. 8). Air parcels that were located near Moscow at 0000 UTC 13 July originated well upstream over western Europe and the North Atlantic 120 h earlier (Fig. 8a). These air parcels rapidly moved eastward and were ingested into the circulation of the anticyclone. The air parcels in the middle and upper troposphere descended and cooled, likely because of radiative effects (Figs. 9a,b). The air parcels in the lower troposphere descended and warmed as they circulated anticyclonically while passing near Moscow by 14 July (Figs. 8a, 9a,b). The parcels then rapidly ascended and moved downstream over north-central Asia by 18 July. The trajectory analysis centered on 13 July

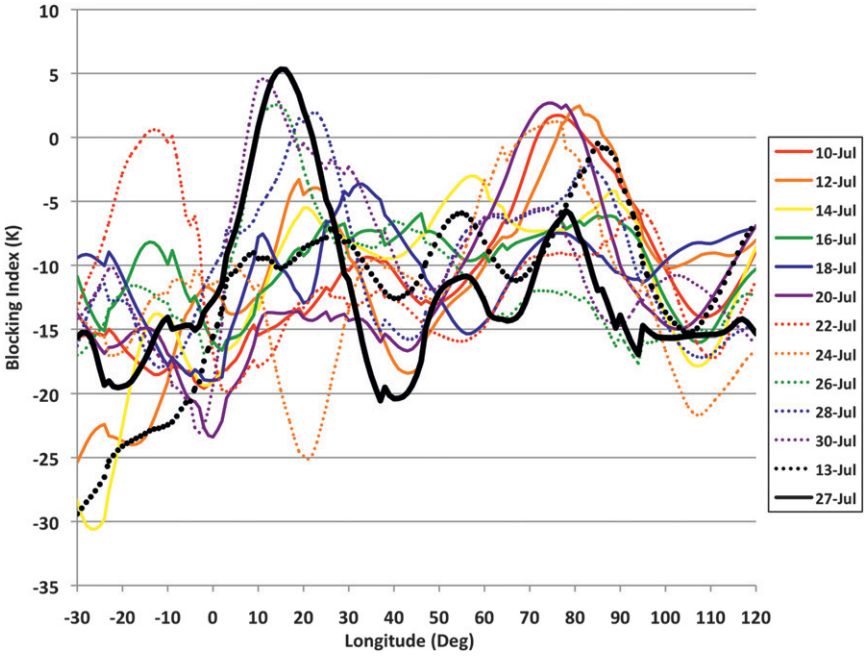

FIG. 7. The blocking index (K) is defined as the meridional difference in potential temperature on the dynamic tropopause as described in Pelly and Hoskins (2003), computed at 0000 UTC 10–30 Jul 2010. Contour lines are defined in the key at the right. Flow is considered blocked when the blocking index is >0.

occurred during a period of temporary weakening and retrogression of the anticyclone (Fig. 6), and is illustrated by the ingestion and rapid ejection of air parcels during this period when the blocking index was <0 (Fig. 7).

Air parcels that originated at 1440 and 3000 m near Moscow on 27 July show an extended period of gradual descent and warming overall (radiative cooling still dominant in the middle troposphere), and recirculation around the blocking anticyclone throughout the 10-day period of analysis (Figs. 8b, 9c,d). The recirculation of air parcels coincides with rapid strengthening of the blocking anticyclone (blocking index >0 between 10° and 40°E after 22 July) and intensification of the closed anticyclonic circulation by 27 July (Figs. 6, 7). The recirculation of air parcels and enhanced dynamically driven subsidence in conjunction with the strengthening anticyclone contributed to the most intense heat over Moscow observed during 28–29 July (Fig. 1), likely further enhanced by land surface feedbacks in the heat wave/drought region, as discussed by Dole et al. (2011).

Air parcels located over northern Pakistan on 27 July originated within the boundary layer over Bangladesh, the Bay of Bengal, and in the monsoon southwesterlies over the Arabian Sea 120 h earlier (Fig. 8b). These air parcels moved northwestward along the southern flank of the Himalayas before rapidly ascending over northern Pakistan by 0000 UTC 27 July (Figs. 8b, 9e,f). Once the air parcels reached jet level, they continued rapidly eastward along the northern flank of the Tibetan anticyclone (Figs. 8b, 10). The behavior of these air parcels over Pakistan shows that boundary layer air rapidly ascended to jet level, likely contributing to jet intensification through vertical potential vorticity (PV) redistribution in response to diabatic heating (e.g., Hoskins et al. 1985), and these air parcels were then quickly carried downstream (note that the warming of air parcels in Fig. 9f was likely related to diabatic heating). The trajectories shown here offer no clear evidence that air parcels associated with convection over northern Pakistan are connected with air parcels undergoing descent in the blocking anticyclone. Additionally, the high-latitude position of the anticyclonic circulation, the apparent wave source region over the northeast Atlantic, and eastward propagation of wave energy also make a Rossby wave–like response forced from the Indian Ocean/Asian monsoon region (e.g., Rodwell and Hoskins 1996) highly unlikely in explaining the blocking pattern over northeastern Europe and western Russia. The key linkage is that the blocking pattern over Europe and Russia and attendant downstream energy dispersion acted to lock in and amplify the upper-level trough northwest of Pakistan and anticyclone over the Tibetan Plateau. The importance of the Pakistan trough and Tibetan anticyclone in the intensification of the upper-level

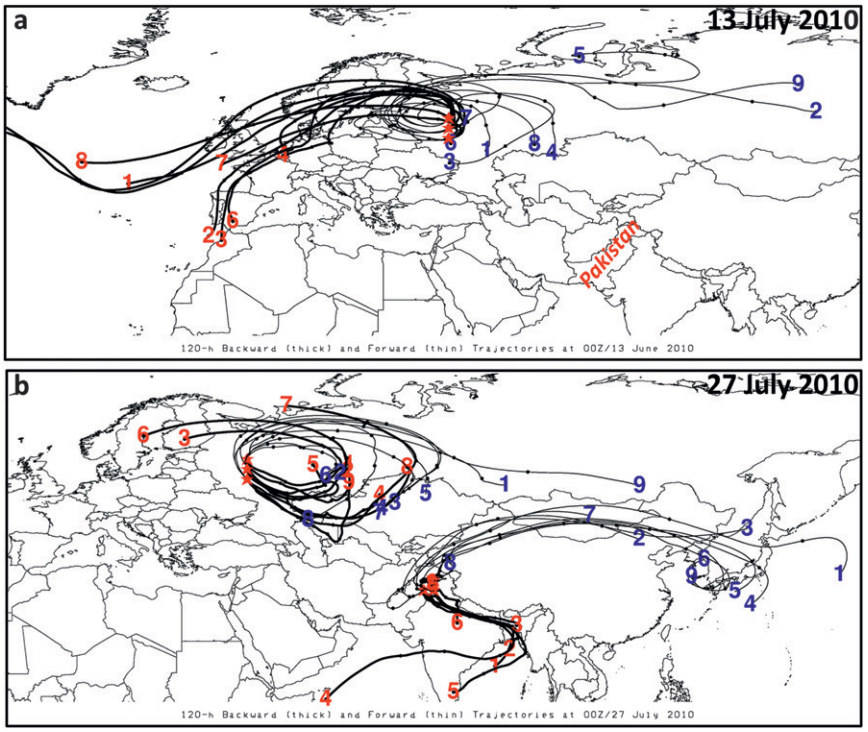

FIG. 8. Nine 120-h backward (thick lines) and forward (thin lines) air parcel trajectories starting at 0000 UTC (a) 13 and (b) 27 Jul 2010. Air parcel trajectory starting locations are indicated by a red star, and the trajectory number is indicated at the ending locations. Trajectories 1, 4, and 7 start at 1440 m MSL; 2, 5, and 8 at 3000 m MSL; and 3, 6, and 9 at 5000 m MSL.

jet over northern Pakistan will be explored in the next section.

5. Tropical–extratropical interaction and upper-level jet intensification

The previous section discussed the linkage between the blocking anticyclone over Russia, trough over northern Pakistan, and anticyclone over the Tibetan Plateau. This section will explore the intensification of the upper-level jet over northern Pakistan. While the amplification of the synoptic-scale pattern appears to be primarily driven by downstream energy dispersion in midlatitudes, we will explore the contribution of tropical–extratropical interaction in pattern amplification and jet intensification. By 0000 UTC 28 July, an extremely amplified pattern was in place over much of western and central Asia (Fig. 10). A +2.0–3.0-σ blocking anticyclone was anchored over western Russia (see also Fig. 7), with a −1.0- to −2.0-σ trough northwest of Pakistan and a +2.0–3.0-σ anticyclone over the Tibetan Plateau. A 37.5 m s^{-1} jet was located northwest of Pakistan on the forward flank of the upper-level trough.

The time series of 300-hPa geopotential height and temperature standardized anomalies centered on the Tibetan anticyclone indicate that the anticyclone was most robust during the latter part of July (Fig. 11a). The time series of 300-hPa wind speed just northwest of Pakistan shows that the upper-level jet was also most intense during the latter part of July (Fig. 11b). The Tibetan anticyclone and upper-level jet northwest of Pakistan were not as robust for previous rain events during June and July. The increased intensity of these two features likely contributed to the extreme nature of the 27–30 July rain event. Additionally, persistent tropospheric-deep anomalous easterly flow developed over northern India on the southern flank of the Tibetan anticyclone by 26 July (Figs. 11c,d). The deep easterly flow, which was not present during previous rain events over northern Pakistan in June and July, facilitated the westward advection of deep tropical monsoon moisture from Bangladesh to northern Pakistan as shown by the trajectory analysis (Fig. 8b).

The intensification of the upper-level jet northwest of Pakistan occurred in conjunction with the interaction of tropical and extratropical processes. To illustrate the nature of the tropical–extratropical interaction, we have constructed a sequence of (i) 200-hPa streamfunction, PV, advection of PV by the nondivergent wind, and wind speed, and (ii) 200-hPa irrotational wind, PV,

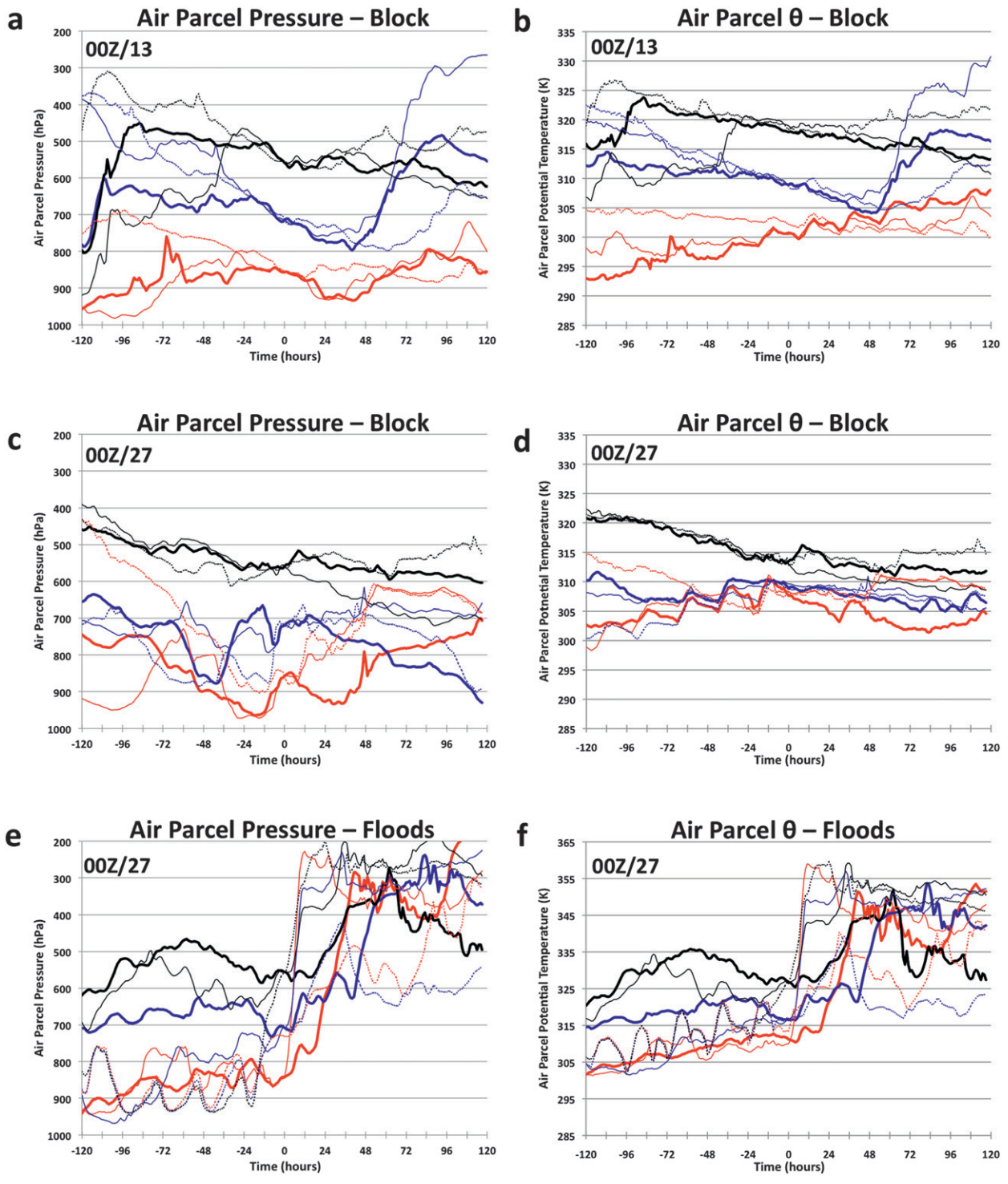

FIG. 9. Time series of air parcel pressure (hPa) and potential temperature (K) are shown for parcel trajectories over Russia on (a),(b) 13 and (c),(d) 27 Jul, and (e),(f) over Pakistan on 27 Jul 2010. Individual trajectories correspond to trajectories plotted in Fig. 8, and are indicated as follows: 1: red thick solid line, 2: blue thick solid line, 3: black thick solid line, 4: red thin solid line, 5: blue thin solid line, 6: black thin solid line, 7: red thin dashed line, 8: blue thin dashed line, and 9: black thin dashed line.

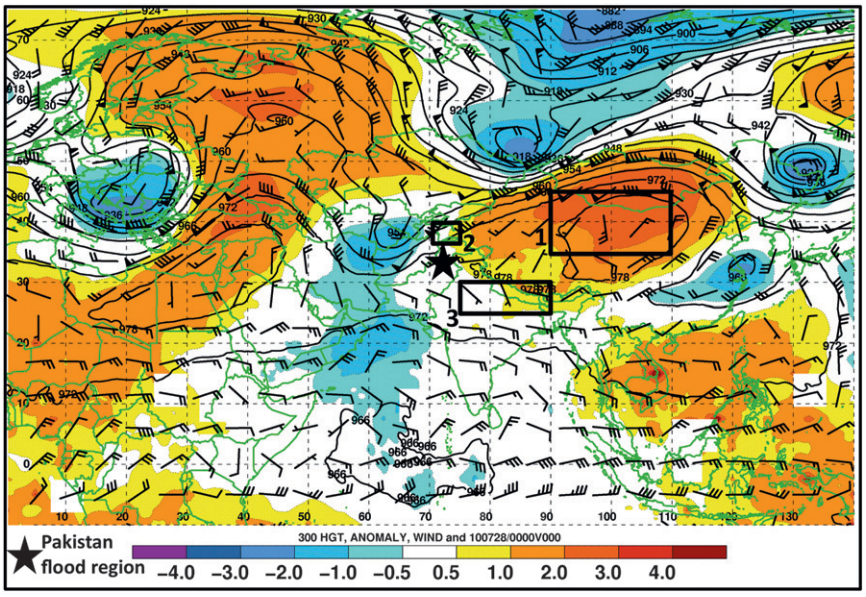

FIG. 10. The 300-hPa geopotential height (solid contours every 6 dam), standardized anomaly (shaded in σ), and wind (barbs as in Fig. 4) at 0000 UTC 28 Jul 2010. The anomaly was computed using the long-term (1979–2009) 21-day running mean. The Pakistan flood region is marked with a star and averaging boxes for the parameters shown in Fig. 11 are indicated.

relative humidity, and 600–400-hPa-layer-average vertical motion charts for 0000 UTC 21, 24, and 27 July (Fig. 12). In a general sense, the former synoptic chart illustrates the contribution of extratropical forcing, while the latter chart constitutes the tropical forcing. At 0000 UTC 21 July, the subtropical anticyclone is anchored over the Middle East, with a zonally oriented 30–35 m s^{-1} subtropical jet stretching along 40°N toward the Tibetan Plateau (Figs. 12a,b). By 0000 UTC 24 July, downstream amplification of the subtropical flow resulted in anticyclogenesis over the Tibetan Plateau (Figs. 6, 12c) and intensification of the upper-level jet northwest of Pakistan to 60 m s^{-1} (Fig. 12d). Intensification of the upper-level jet was likely a result of tropical–extratropical interaction, manifested as positive PV advection by the nondivergent wind on the cyclonic shear side of the jet northwest of Pakistan (Fig. 12c), and inferred negative PV advection by the irrotational wind on the anticyclonic shear side of the jet (Fig. 12d). The former extratropical ''forcing'' is related to the persistent upper-level trough northwest of Pakistan, while the latter tropical forcing is related to increased upper-level outflow in conjunction with a broad region of organized convection over and just east of the Bay of Bengal and over Bangladesh and northeast India. By 0000 UTC 27 July, the upper-level jet northwest of Pakistan intensified to nearly 70 m s^{-1} in response to continued positive PV advection on the cyclonic shear side of the jet and large-scale outflow from tropical convection over northern India and the Bay of Bengal on the anticyclonic shear side of the jet (Figs. 12e,f; see also Figs. 8b, 9f).

The organized convection over the Bay of Bengal and northern Bangladesh and India during 24–27 July appears to be associated with the MJO, which moved eastward across the Indian Ocean during the latter part of July (Fig. 13a). The broad time-mean outflow associated with the MJO was likely an important contributor to anticyclogenesis over the Tibetan Plateau and upper-level jet intensification northwest of Pakistan, in addition to extratropical downstream development (Fig. 13b). The contribution of upper-level jet intensification from an intense MJO during the latter part of July was the missing ingredient during previous heavy rain events during June and July that occurred in conjunction with a weaker, more zonal, upper-level jet (Figs. 11a,b). Tropical–extratropical interaction during the later part of July likely turned what would have been a rain event comparable to previous events in June and July into a historic rain event.

6. Role of a monsoon depression and barrier jet in the flux of moisture into northern Pakistan

a. Synoptic-scale evolution and structure

Figure 14 shows the evolution of the 200- and 700-hPa flow fields and column-integrated precipitable water (PW) for 26–28 July (see also Houze et al. 2011, 292–295). At 0000 UTC 26 July, deep tropical moisture with

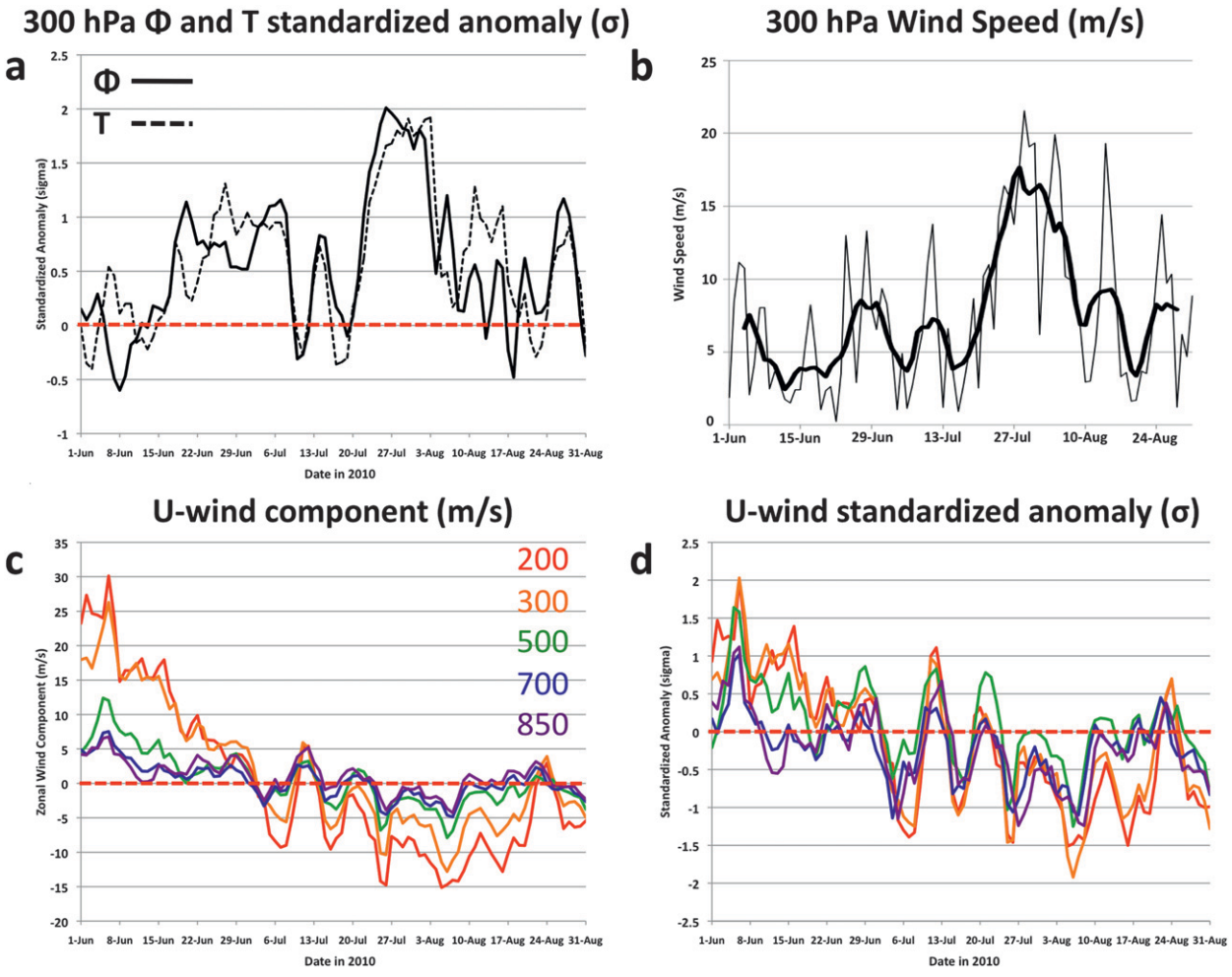

FIG. 11. Time series of (a) 300-hPa geopotential height (solid line) and temperature (dashed line) standardized anomaly (σ), (b) 300-hPa wind speed (thin line; m s^{-1}) and 5-day running mean (thick line), (c) zonal wind component (m s^{-1}), and (d) zonal wind component anomaly (σ). The parameters in (a) are averaged over box 1 shown in Fig. 10, in (b) over box 2 in Fig. 10, and in (c),(d) over box 3 in Fig. 10. The zonal wind components in (c),(d) are computed at 200 (red line), 300 (orange line), 500 (green line), 700 (blue line), and 850 (purple line) hPa.

total column PW values above 65 mm was in place over northern India just south of the Himalayas (Fig. 14a). The tropical moisture was embedded in deep easterly flow (Fig. 11), with a region of enhanced moisture near the India–Pakistan border where PW values exceeded 70 mm (Figs. 14a,b). The deep easterly flow was manifested by the anticyclonic easterly flow on the equatorward flank of the Tibetan anticyclone, and at low levels by enhanced southeasterly flow on the poleward flank of a monsoon depression over eastern India. By 0000 UTC 27 July, the deep tropical moisture with PW values > 70 mm moved westward into Pakistan (Fig. 14c) as the 700-hPa flow veered from northeasterly to weak easterly in response to the movement of the monsoon depression to western India and extreme southeast Pakistan (Figs. 14b,d). Nearly 30 mm of rainfall occurred over parts of northern Pakistan on 27 July (Fig. 2a) as this deep tropical moisture moved beneath the equatorward jet entrance region of the 200-hPa jet in the presence of weak upslope flow at 700 hPa (Figs. 14c,d).

Over 100 mm of rainfall occurred over northern Pakistan on 28 July (Fig. 2b) as deep tropical moisture continued to surge into Pakistan beneath the equatorward entrance region of the 200-hPa jet (Figs. 4, 14e). Additionally, the core of an intense low-level jet on the poleward side of the monsoon depression moved from north-central India at 0000 UTC 27 July into northern Pakistan by 0000 UTC 28 July, resulting in the development of intense (>15 m s^{-1}) moist upslope flow (Figs. 14d,f). The deep southeasterly flow at 0000 UTC 28 July was driven by the deep anomalous easterly flow on the equatorward flank of the Tibetan anticyclone and enhanced southeasterly low-level

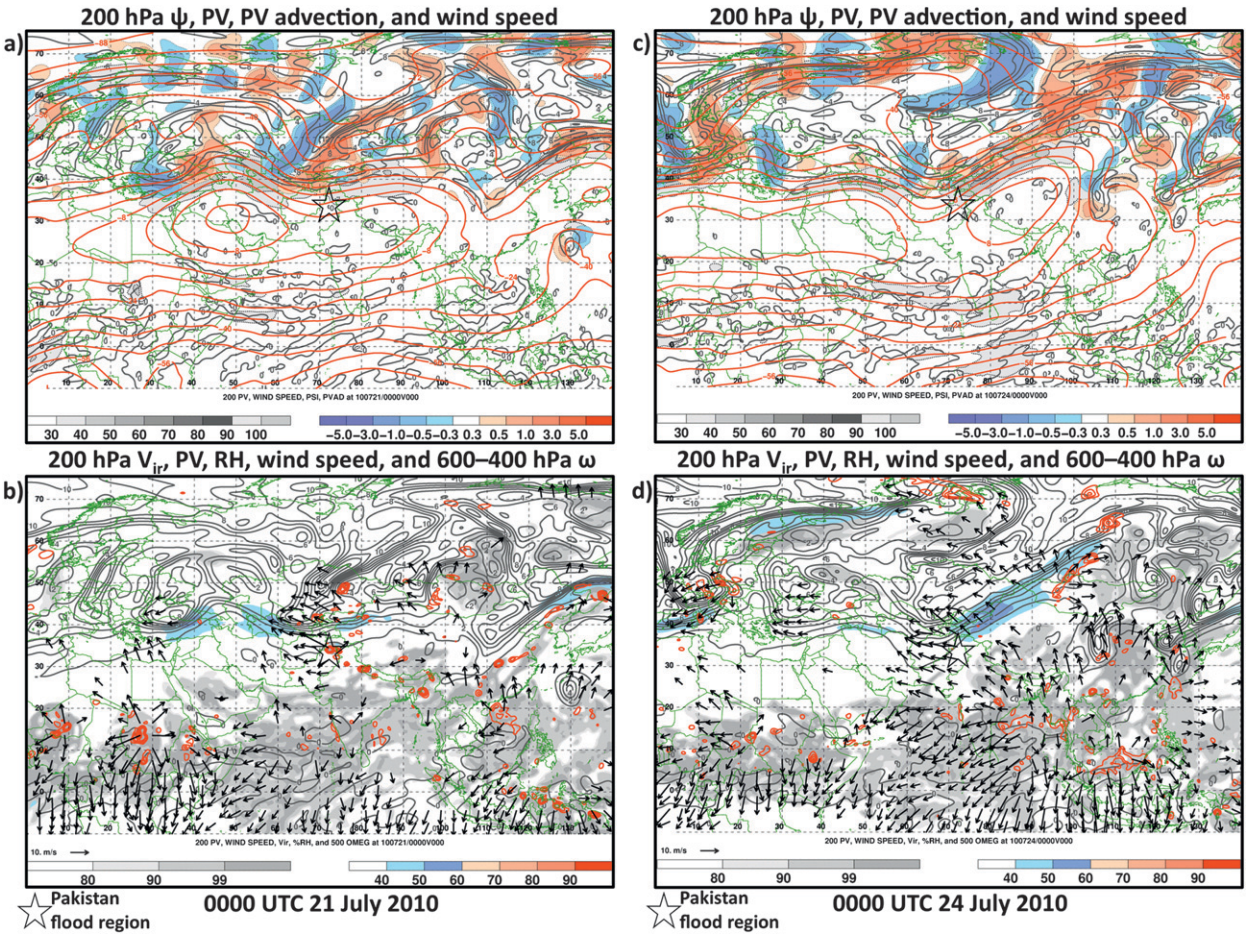

FIG. 12. Analysis at 0000 UTC 21 Jul 2010 of (a) 200-hPa streamfunction (solid red contours every 8.0×10^6 m^2 s^{-1}), PV [solid gray contours every 2.0 PV units (PVU; 1.0 PVU = 1.0×10^{-6} m^2 s^{-1} K kg^{-1})], PV advection by the nondivergent wind (shaded according to the color bar in 10^{-10} PVU s^{-1}), and wind speed (shaded according to the grayscale in m s^{-1}), and (b) 200-hPa irrotational wind (arrows $\geq$5.0 m s^{-1}), PV (solid gray contours every 1.0 PVU), relative humidity (shaded according to the grayscale in %), wind speed (shaded according to the color bar in m s^{-1}), and 600–400-hPa-layer-average ascent (solid red contours every 5.0×10^{-3} hPa s^{-1} starting at -5.0×10^{-3} hPa s^{-1}). (c),(d) As in (a),(b), respectively, but for 0000 UTC 24 Jul 2010. (e),(f) As in (a),(b), respectively, but for 0000 UTC 27 Jul 2010. The Pakistan flood region is marked by a star.

jet on the poleward flank of the westward-moving monsoon depression. The coupling of the intense low-level jet with the upper-level equatorward jet entrance region was likely key to producing robust synoptic-scale ascent that helped drive the long-lived episode of convection over northern Pakistan on 28–29 July.

b. *Barrier jet structure and moisture source regions*

Vertical cross sections at 0000 UTC 28 July—the beginning of the period of heaviest rain over northern Pakistan—tangent and normal to the low-level jet are presented in Fig. 15. The along-jet vertical cross section shows the presence of tropical moisture through a deep layer embedded in tropospheric deep easterly flow (Fig. 15a) on the equatorward flank of the Tibetan anticyclone (Fig. 10). Note that the low-level southeasterly flow was enhanced below ~600 hPa (marked "B"). The low-level jet was instrumental in advecting tropical moisture to the high terrain of northern Pakistan [confirming the notions of Houze et al. (2011)], as illustrated by the layer-average 850–700-hPa moisture flux averaged on 28–29 July (Fig. 16), where robust upslope flow was observed (Figs. 15a, 16). Both the moisture flux and trajectory analyses show that the low-level moisture originated over the Bay of Bengal and in the monsoon southwesterlies (Figs. 8b, 16). Deep ascent that occurred in conjunction with the upslope flow and attendant convection over northern Pakistan was located within the equatorward entrance region of the upper-level jet (marked "A"). The coupling of the upper-level jet and low-level jet was instrumental in facilitating

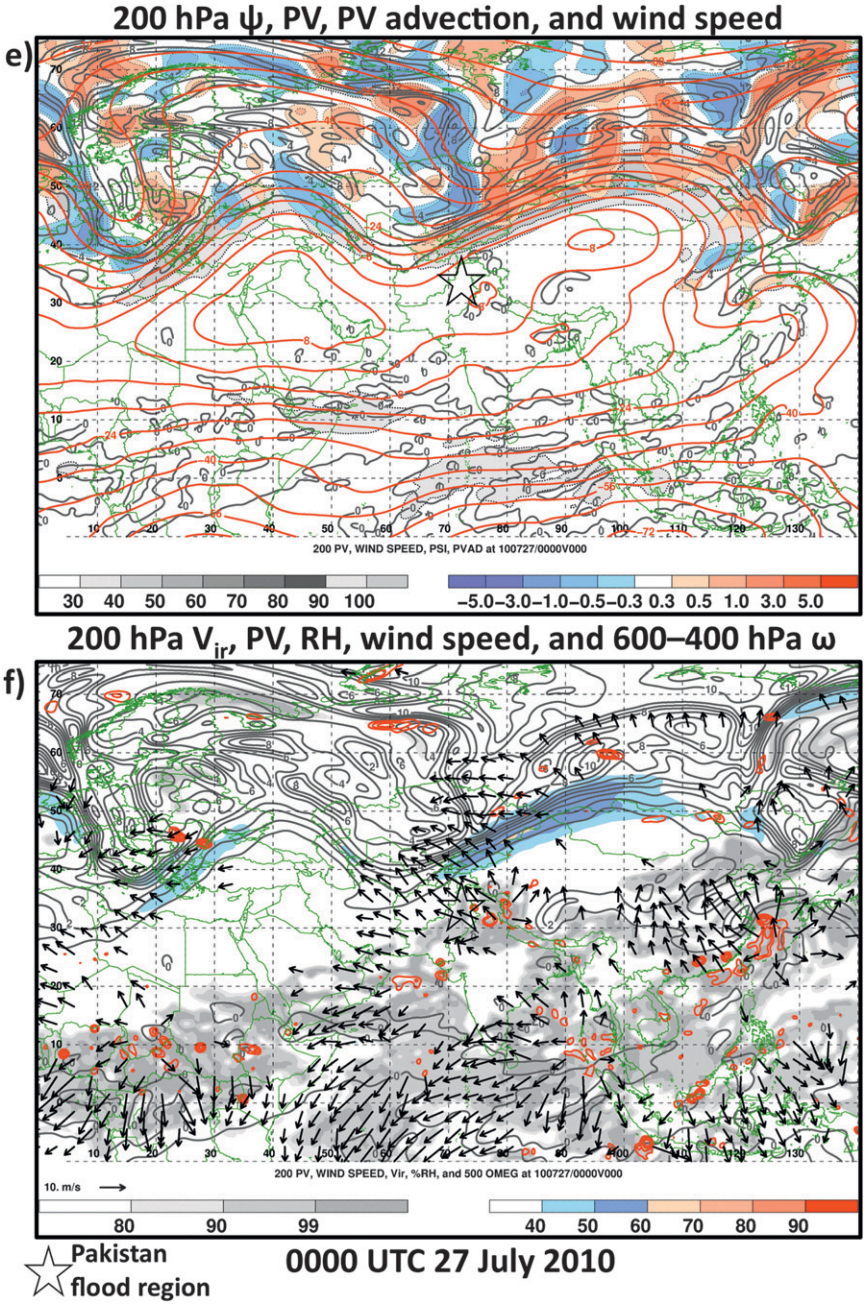

FIG. 12. (*Continued*)

synoptic-scale ascent during the latter part of July, contributing to the long-lived episode of active convection (Fig. 3).

The vertical cross section oriented normal to the low-level jet at 0000 UTC 28 July shows how the low-level jet (labeled ''C'') is most intense adjacent to the Himalayan barrier and resembles the well-studied classical barrier jets seen along the U.S. West Coast (e.g., Olson et al. 2007), Appalachian Mountains (e.g., Bell and Bosart 1988), Alps (e.g., Chen and Smith 1987), and over Taiwan (e.g., Li and Chen 1998). Barrier jets typically form when flow on the upstream side of a mountain barrier is blocked, producing a pressure gradient component parallel to the barrier. The wind can then accelerate down the along-barrier pressure gradient producing a barrier jet. During 25–28 July, the Froude number $F_r = U/(Nh)$ (where U is the low-level wind speed normal to the mountain barrier, h is the terrain height, and N is the Brunt–Väisälä frequency) values

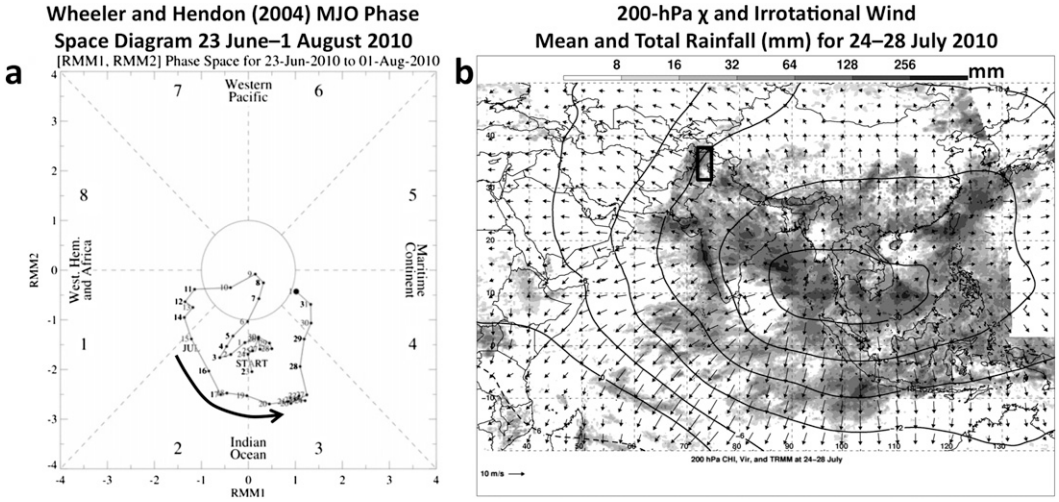

FIG. 13. (a) MJO phase space diagram for 23 Jun–1 Aug 2010 based on Wheeler and Hendon (2004) (source: NCEP Climate Prediction Center website). (b) Time-mean 200-hPa velocity potential (solid contours every 3.0×10^6 m^2 s^{-1}), irrotational wind (arrows in m s^{-1}), and TRMM-derived total rainfall (shaded in mm) for 24–28 Jul 2010.

along the southern flank of the Himalayas ranged from 0.1 to 0.2 (computed from proximity soundings; see also Fig. 4), indicating that cyclonic flow around the monsoon depression moving westward across central India was blocked when it encountered the Himalayas, setting the stage for barrier jet formation. While we refer to the low-level jet as a barrier jet for the remainder of this manuscript because of its resemblance to previously studied barrier jets (e.g., Olson et al. 2007), it is realized that the relatively coarse resolution of the gridded datasets used here does not have the proper resolution in time and space to diagnose (e.g., through a momentum budget) the mechanisms for barrier jet formation. A high-resolution numerical simulation, an avenue of future work, may be able to more definitively determine whether the low-level jet depicted here is a true barrier jet.

The importance of the southeasterly barrier jet in driving heavy rainfall is summarized in the time series of lift, instability, and moisture parameters for 15–31 July 2010 shown in Fig. 17. These parameters were area-averaged in the dashed box shown in Fig. 16 located on the eastern flank of the heavy rainfall region. Note that throughout 15–31 July, the 850-hPa u-wind component was westerly (i.e., downslope) over northeast Pakistan except when the barrier jet was present and induced easterly (i.e., upslope) flow (Figs. 14f, 17a). The easterly upslope flow contributed to a marked increase in (i) PW to near 50 mm through moisture advection in agreement with moisture flux and air parcel trajectory analyses (Figs. 8b, 16), (ii) relative humidity in the 700–500-hPa layer to near 90% through moisture advection throughout a deep layer in conjunction with the deep easterly flow on the equatorward flank of the Tibetan anticyclone and forced ascent through low-level upslope flow, and (iii) convective available potential energy (CAPE) to near 800 J kg^{-1} through deep-layer moistening and destabilization. The evolution of these parameters illustrates how all the necessary ingredients—lift, instability, and moisture—were in place for heavy rain and flooding to occur, in agreement with the findings of Houze et al. (2011).

7. Ensemble analysis

Given the historical, high-impact nature of the heavy rain event over Pakistan on 27–30 July 2010, the forecast performance for this event is of significant interest. Webster et al. (2011) examined quantitative precipitation forecasts (QPFs) from the ECMWF EPS for northern Pakistan during July–August and found that the multiple rain events (Fig. 1), or monsoon pulses, were predictable with a high probability 6–8 days in advance (see also Ghelli et al. 2010). The result from Webster et al. (2011) motivates the further use of ECMWF EPS forecasts to determine synoptic-scale features that modulated the production of heavy rainfall, following methods similar to those shown in Hakim and Torn (2008).

The probability of precipitation (POP) >50 mm during 28–29 July at decreasing lead times is shown in Fig. 18. In agreement with the analysis shown in Webster et al. (2011), the ECMWF EPS shows POP forecasts reaching 60% over northern Pakistan in the 96–144-h forecast initialized at 0000 UTC 24 July (Fig. 18a). The region of highest POP over northern Pakistan agrees with the observed TRMM-derived precipitation analysis. POP

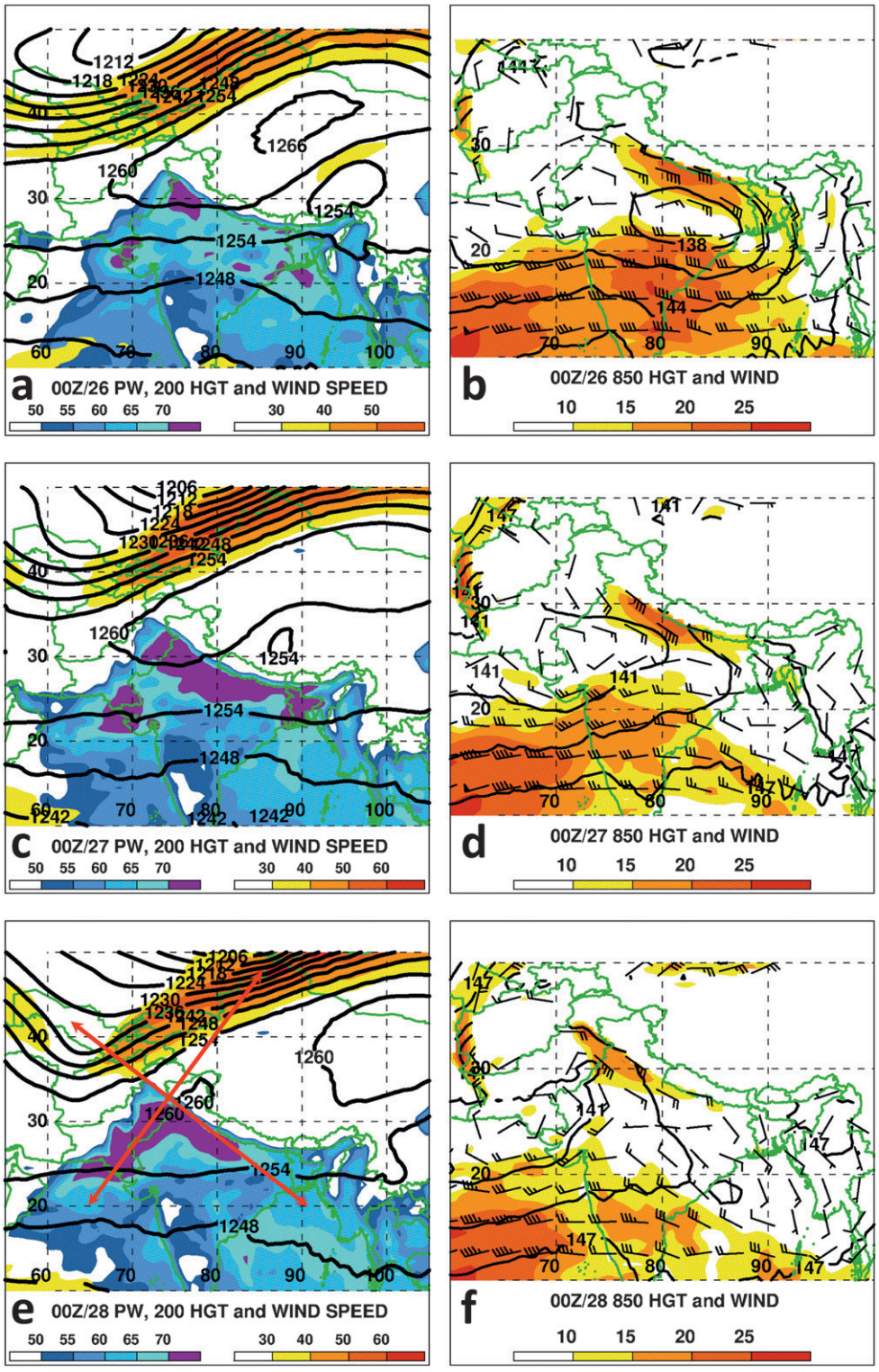

FIG. 14. Total column PW (shaded according to the lower left color bar in mm) and 200-hPa geopotential height (solid contours every 6 dam) and wind speed (shaded according to the lower right color bar in m s^{-1}) at 0000 UTC (a) 26, (c) 27, and (e) 28 Jul 2010. The 850-hPa geopotential height (solid contours every 3 dam), wind (barbs as in Fig. 4), and wind speed (shaded according to the color bar in m s^{-1}) at 0000 UTC (b) 26, (d) 27, and (f) 28 Jul 2010. Cross-sectional orientations for Fig. 15 are illustrated in (e).

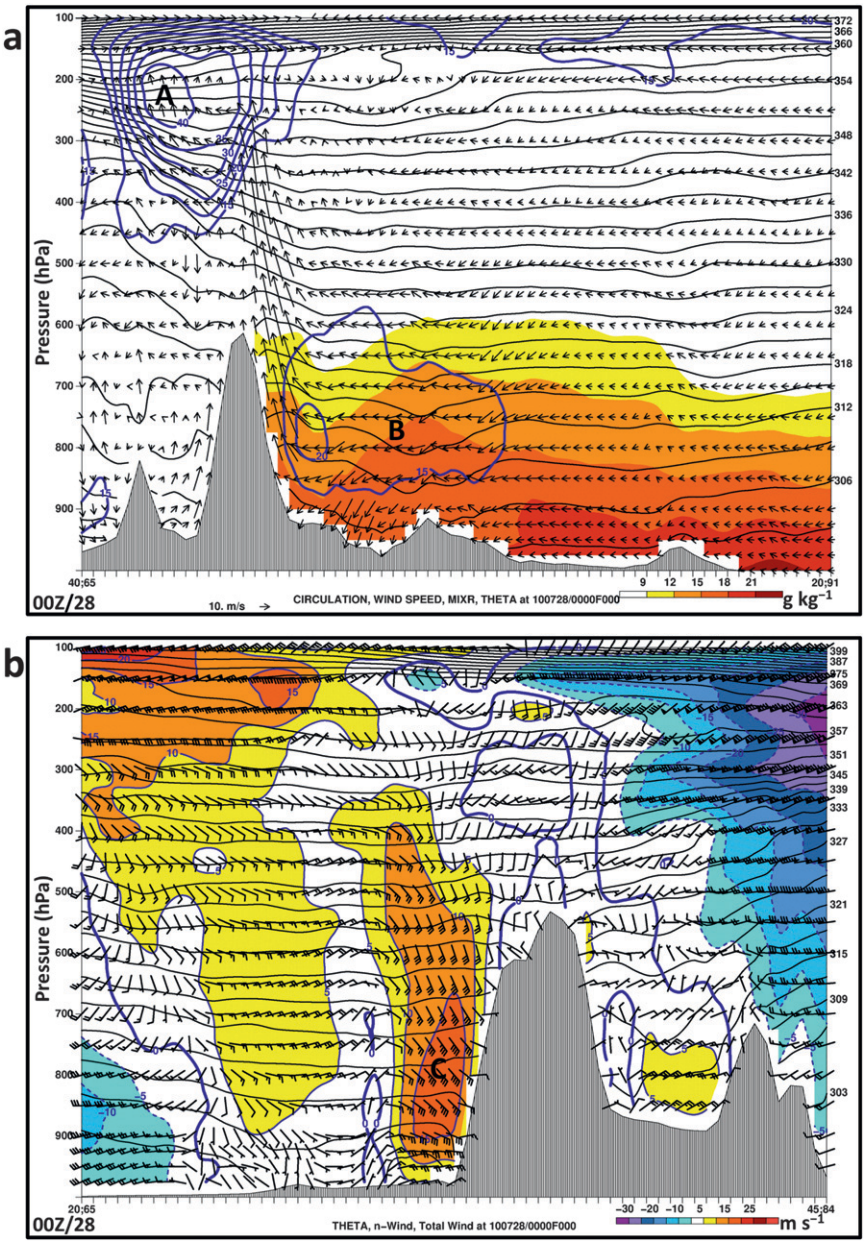

FIG. 15. Vertical cross section at 0000 UTC 28 Jul 2010 of (a) mixing ratio (shaded according to the color bar in g kg^{-1}), flow in the plane of the cross section (arrows in m s^{-1}), wind speed (blue contours every 5 m s^{-1} starting at 5.0 m s^{-1}), and potential temperature (solid thin black contours every 3 K), and (b) wind component normal to the cross section (blue contours every 5 m s^{-1} and shaded according to the color bar; solid contours >0, dashed contours <0), potential temperature (solid thin black contours every 3 K), and wind (barbs as in Fig. 4). Cross-sectional orientations are marked in Fig. 14a. The core of the upper-level jet and low-level barrier jet are marked by A and B, respectively, in (a). The core of the low-level barrier jet is marked C in (b).

forecasts along the southwest coast of India were in good agreement with observations as well, with less agreement along the southeast coast of India (Fig. 18a). POP forecasts became more focused and increased markedly with decreasing lead time, with over 90% POP >50 mm forecasted over northern Pakistan by the 0000 UTC 27 July initialization for 28–29 July (Figs. 18b–d). By the 0000 UTC 28 July initialization, the ECMWF EPS has over 90% POP >50 mm throughout the northern Pakistan region (Fig. 18e).

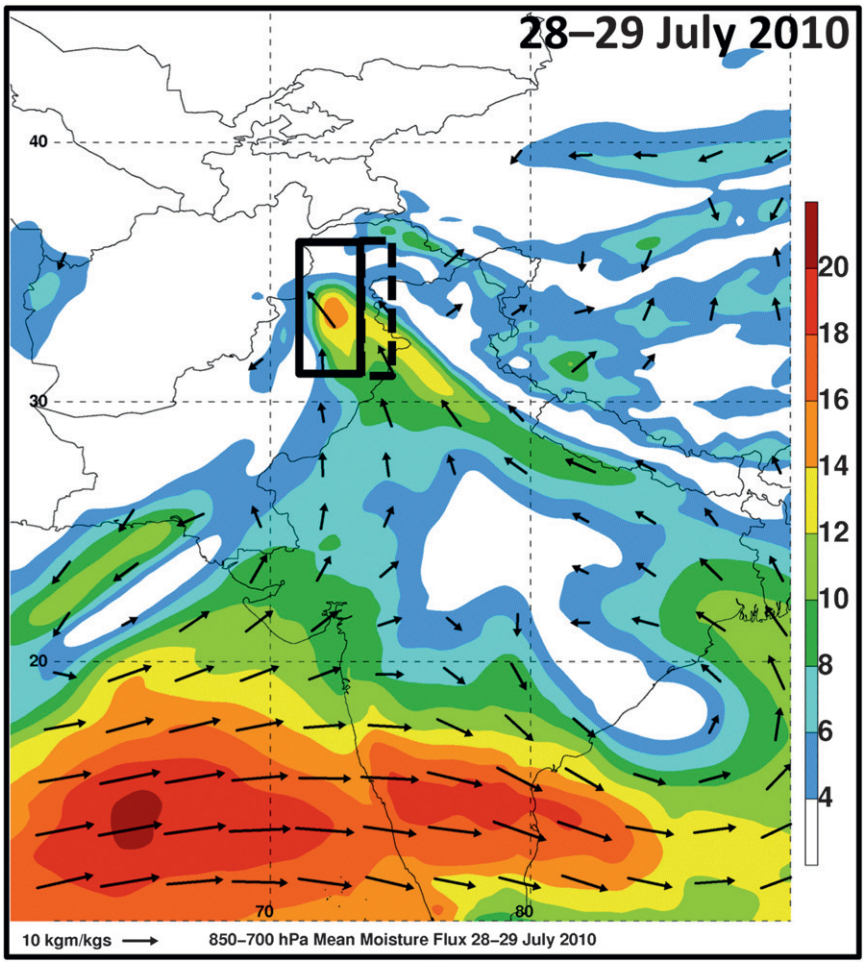

FIG. 16. Layer-average moisture flux (arrows in kg m kg^{-1} s^{-1}; magnitude is shaded according to the color bar in kg m kg^{-1} s^{-1}) in the 850–700-hPa layer time averaged for 28–29 Jul 2010. The dashed box marks the region of averaging for the parameters shown in Fig. 17, except for the TRMM rainfall, which is averaged over the solid box.

The POP forecasts of >100 mm of rainfall show similar evolution at decreasing lead times to POP forecasts of >50 mm (Fig. 19). The 96–144-h forecast initialized at 0000 UTC 24 July shows a broad region of 4% (corresponding to two ECMWF EPS members) with a more focused region of 10% over northern Pakistan (Fig. 19a). The POP forecasts >100 mm increased markedly, reaching 40% by the 0000 UTC 26 July, 80% by the 0000 UTC 27 July, and over 90% by the 0000 UTC 28 July initialization (Figs. 19b–e). The ECMWF EPS POP forecasts were all in good agreement with the observed region of >100 mm of rainfall for 28–29 July.

Since the 96–144-h QPF initialized at 0000 UTC 24 July did a reasonable job of indicating that a heavy rain event was possible over northern Pakistan on 28–29 July, and the lead time was long enough for sufficient spread in the ensemble (not shown), it is useful to compare ''wet'' and ''dry'' ensemble members. Examination of composite fields of the wet and dry ensemble members provides insight on the key synoptic-scale features associated with heavy rainfall. The top 10 wet and dry members were determined by computing the area-average 48-h rainfall forecasted during 28–29 July (see averaging box in Fig. 2a). Composite geopotential height and wind fields were then computed for the 96-h forecast initialized at 0000 UTC 24 July for the wet and dry ensemble groups for comparison (Fig. 20). The distribution of rainfall for the 51 ensemble members was roughly normal with a mean rainfall of 22.2 mm (not shown). The 10 dry ensemble members produced a mean 48-h area-average rainfall of 12.9 mm (ranging from 9.6 to 15.1 mm), while the 10 wet members produced 31.5 mm (26.8–39.6 mm). Note that the QPF, while excellent in areal coverage, underforecasted the

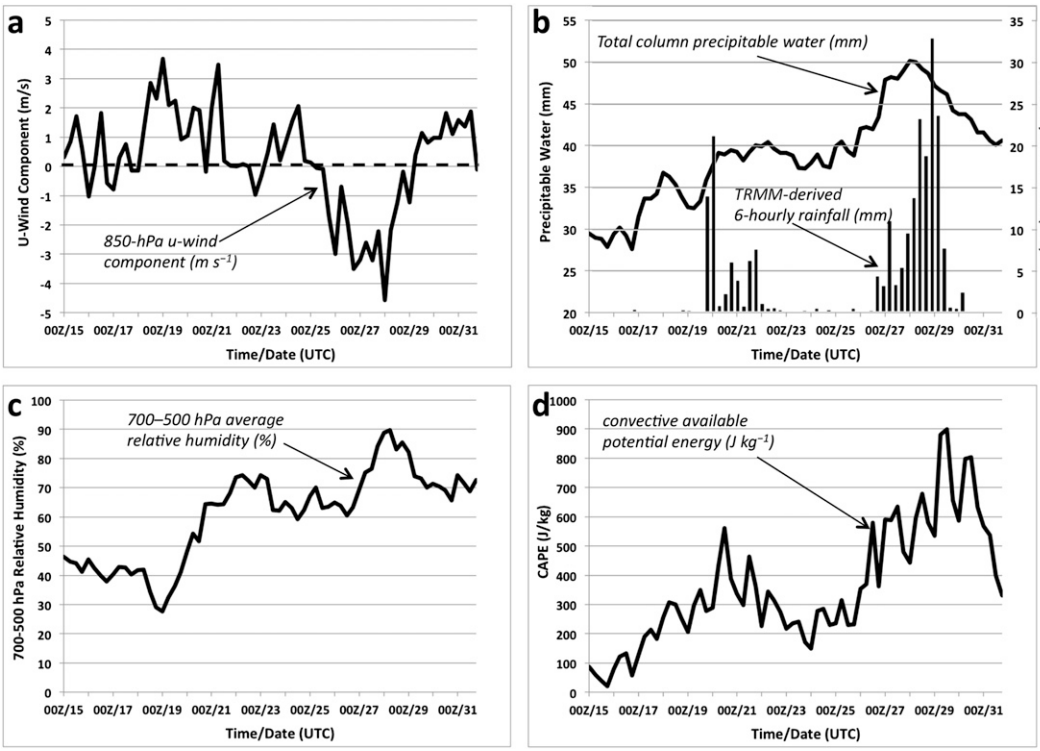

FIG. 17. Time series of (a) 850-hPa u-wind component (m s^{-1}), (b) total column PW (mm) and TRMM-derived 6-hourly rainfall (mm), (c) 700–500-hPa-layer-average relative humidity (%), and (d) CAPE (J kg^{-1}) for 15–31 Jul 2010. The TRMM-derived rainfall was averaged within the solid box plotted in Fig. 16 while all other parameters were averaged in the dashed box plotted in Fig. 16. CAPE was computed using the mean air parcel in the lowest 500 m above ground level.

rainfall amounts quite dramatically as 129.6 mm was observed in 48 h by the TRMM satellite within the same averaging box during 28–29 July. Four of the EPS members did forecast maximum gridpoint values over 250 mm, however, indicating ~8% probability of an extreme high-end rainfall event in localized regions.

The 200-hPa geopotential height ensemble mean and difference between wet and dry ensemble members is shown in Fig. 20a. The ensemble mean shows the extreme eastern flank of the blocking anticyclone over western Russia, the attendant downstream trough northwest of Pakistan, and the anticyclone over the Tibetan Plateau. The difference fields indicate that the pattern was more amplified in the wet ensemble members, with a stronger blocking anticyclone over Russia, and a deeper trough northwest of Pakistan. The positive height difference north of Pakistan and over extreme western China suggests that the Tibetan anticyclone was displaced westward in the wet ensemble members. There is also a signature for lower geopotential heights in the wet members over extreme northern China, Mongolia, and southern Russia. The combination of these lower geopotential heights poleward of higher geopotential heights north of Pakistan indicates that a stronger upper-level jet was in place in the wet ensemble members as indicated by the 200-hPa wind analysis in Fig. 20b.

The 700-hPa geopotential height ensemble mean and difference fields show the southeast flank of the blocking anticyclone over Russia and the monsoon depression over southern Pakistan, western India, and the northern Arabian Sea (Fig. 20c). The difference fields indicate that the monsoon depression is located farther east over western India at 0000 UTC 28 July in the wet ensemble members. The relative eastward displacement of the monsoon depression in the wet members may be related to the enhanced monsoon southwesterly flow over the Arabian Sea and facilitated stronger southeasterly flow over northern India into northern Pakistan, including the signature of a barrier jet–like feature (Fig. 20d).

In summary, the ensemble analysis highlights the important synoptic features relevant to the production of heavy rainfall over northern Pakistan: (i) the amplitude of the upper-level flow pattern, and (ii) the position of the monsoon depression and attendant barrier jet. In the wet ensemble members, the upper-level flow pattern is more amplified compared to the dry members. While

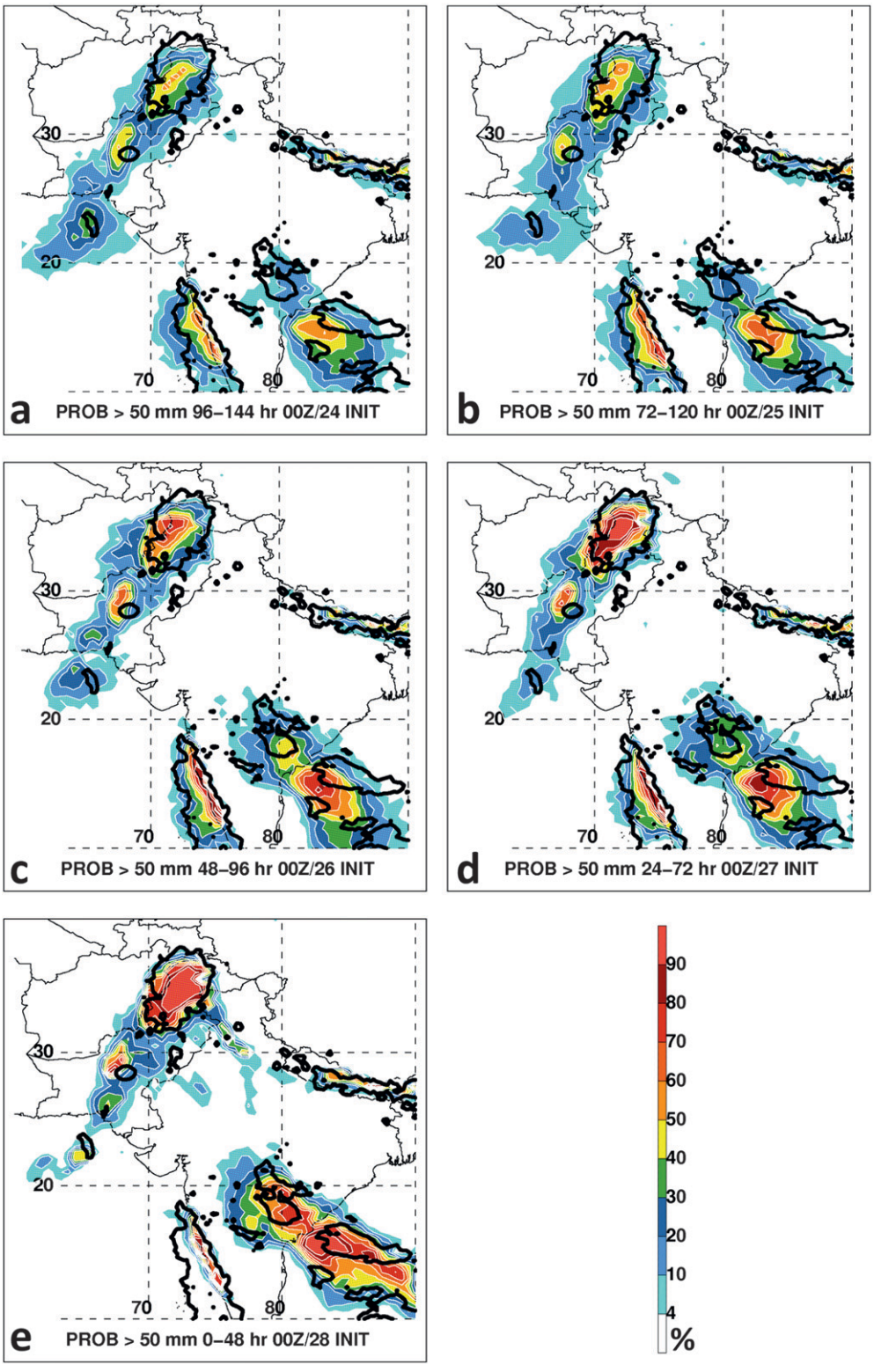

FIG. 18. Raw ECMWF EPS probabilities, at decreasing lead times, of 50 mm of precipitation in the 48-h period between 0000 UTC 28 Jul and 0000 UTC 30 Jul 2010. Probabilities are shaded according to the color bar in %. Regions where at least 50 mm of rainfall was observed in the TRMM dataset are contoured in black. Model initialization times shown are 0000 UTC (a) 24, (b) 25, (c) 26, (d) 27, and (e) 28 Jul 2010.

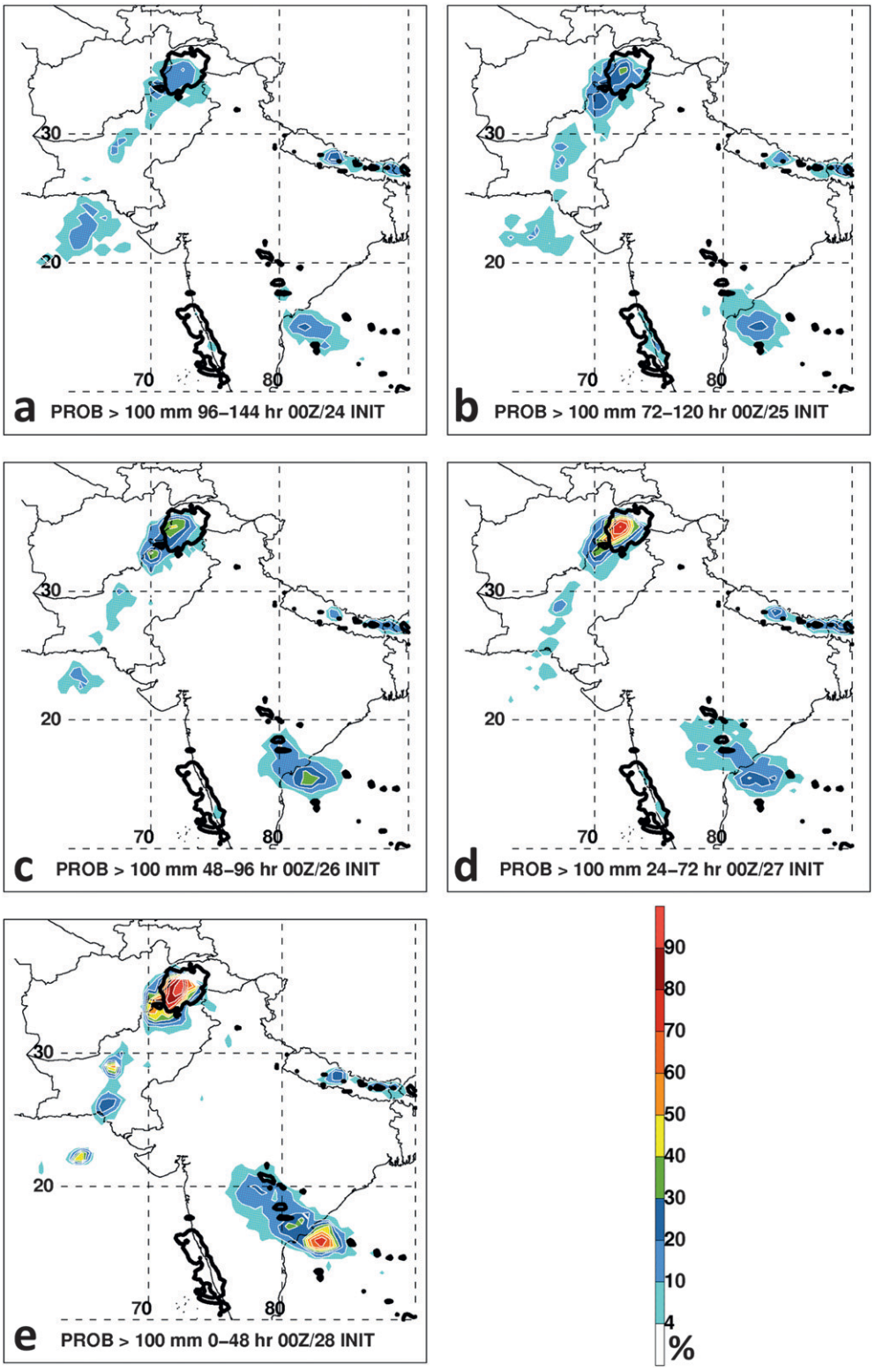

FIG. 19. As in Fig. 18, but for 100 mm of precipitation.

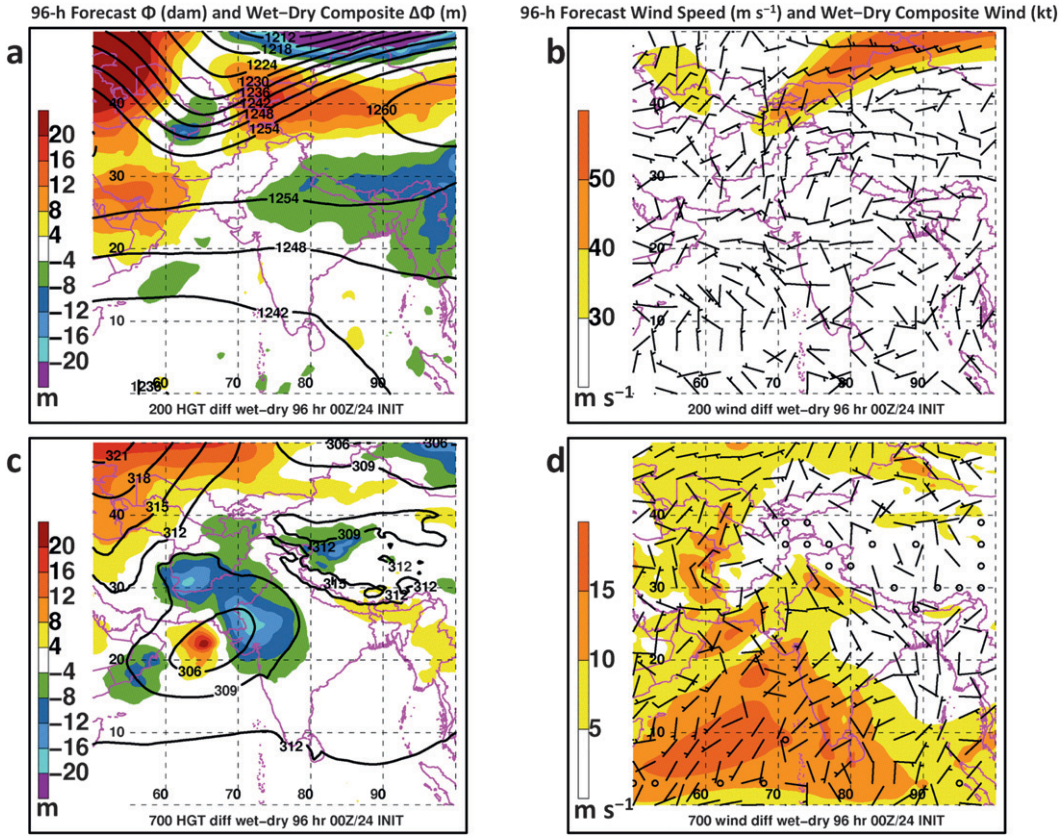

FIG. 20. ECMWF EPS 96-h forecast, initialized at 0000 UTC 24 Jul 2010 verifying 0000 UTC 28 Jul 2010, of (a) ensemble mean 200-hPa geopotential height (solid contours every 6 dam) and height difference between the top 10 wettest and top 10 driest members (''wet'' minus ''dry'') in the ensemble (shaded according to the color bar in m), (b) ensemble mean 200-hPa wind speed (shaded according to the color bar in m s^{-1}) and vector wind difference between the top 10 wettest and top 10 driest members in the ensemble (barbs as in Fig. 4), (c) ensemble mean 700-hPa geopotential height (solid contours every 3 dam) and height difference between the top 10 wettest and top 10 driest members in the ensemble (shaded according to the color bar in m), and (d) ensemble mean 700-hPa wind speed (shaded according to the color bar in m s^{-1}) and vector wind difference between the top 10 wettest and top 10 driest members in the ensemble (barbs as in Fig. 4).

the bulk upscale effect of convection associated with the Pakistan rain event likely affected the upper-level flow structure, it is likely that these effects are not yet fully realized since the ensemble analysis is for the beginning of the heavy rain event. The increased amplitude of the upper-level flow pattern, however, may be a result of downstream amplification from the more intense blocking anticyclone over Russia in the wet ensemble. The more amplified upper-level pattern contributes to a more intense upper-level jet northwest of Pakistan. The position of the monsoon depression over western India is also instrumental in regulating the strength of the southeasterly upslope flow over northern Pakistan; a monsoon depression positioned farther northeast (southwest) is associated with a stronger (weaker) low-level jet. The ability of the individual members in the ensemble to capture the structure and evolution of the two synoptic features discussed above contributed to the successful forecast of the intensity of the rainfall over northern Pakistan in the 96–144-h forecast. Results of this initial ensemble analysis are consistent with those of detailed observational analyses shown earlier.

8. Concluding remarks

This paper reports on the multiscale aspects of an intense heat wave over western Russia and historic rainfall and flooding over northern Pakistan during late July 2010, with an emphasis on the Pakistan flood event. The dynamical linkages between these two weather events were investigated on the large scale, while the physical mechanisms leading to the historic heavy rains and flooding that occurred over northern Pakistan during 27–30 July 2010 were examined in more detail on the

synoptic and mesoscales. In addition, analyses were performed using the ECMWF EPS forecasts of the 27–30 July 2010 heavy rain event to further examine processes contributing to heavy rainfall over Pakistan. The EPS analysis confirmed the results in Webster et al. (2011), but extended their analysis by additionally highlighting the key synoptic features shown here and in previous studies (e.g., Houze et al. 2011) that drove the extreme rain event. The key findings from this work, as shown in the multiscale observational analysis and ensemble modeling study, are outlined in the following paragraphs.

The blocking anticyclone over western Russia and flanking downstream trough northwest of Pakistan were persistent features throughout the summer of 2010. Downstream energy dispersion from source regions over the North Atlantic modulated the structure and intensity of the blocking anticyclone over western Russia, and the downstream trough northwest of Pakistan and anticyclone over the Tibetan Plateau. Downstream energy dispersion was also documented in Hong et al. (2011) and Lau and Kim (2012). The impact of the intensification of the blocking anticyclone over Russia in late July on the culmination of the most intense heat was illustrated by comparing air parcel trajectory analyses on 13 and 27 July. By the end of July, air parcels were allowed to circulate within the blocking anticyclone, a process that was accompanied by enhanced subsidence. The recirculation and sinking of air parcels, likely in addition to land surface feedbacks, has been found to be important in maintaining prior intense heat waves such as in Europe in 2003 (e.g., Galarneau et al. 2008; Black et al. 2004). Our trajectory analysis of the 2010 Russian heat wave supports and adds to the interpretation of, for example, Grumm (2011) and Lau and Kim (2012), by highlighting the importance of circulation around an unusually strong blocking ridge in the intense Russian heat wave.

Throughout June–August 2010, episodic heavy rain events occurred over northern Pakistan, culminating on 27–30 July with the heaviest rainfall episode, ultimately leading to the historic river flooding in the Indus River basin. Downstream energy dispersion from the intensifying blocking anticyclone contributed to trough deepening northwest of Pakistan and anticyclogenesis over the Tibetan Plateau. This result complements the findings in, for example, Hong et al. (2011) and Lau and Kim (2012). Intensification of the upper-level jet over northern Pakistan occurred in conjunction with tropical–extratropical interaction, where the upper-level PV gradient increased in response to positive PV advection by the nondivergent wind on the cyclonic shear side of the jet and inferred negative PV advection by the irrotational wind on the anticyclonic shear side of the jet. Additionally, the air parcel trajectory analysis suggests that diabatic heating in conjunction with convection over northern India and Pakistan also contributed to a reduction in upper-level PV aloft on the anticyclonic shear side of the jet, providing an additional factor that led to jet intensification and reinforcement of the Tibetan anticyclone. Enhanced convective outflow on the anticyclonic shear side of the jet in late July occurred in conjunction with an eastward-propagating MJO across the Indian Ocean. Relating tropical–extratropical interaction, including the direct implication of the MJO, to upper-level jet intensification extends the original findings of Hong et al. (2011) and Lau and Kim (2012), who considered the structure of the upper-level trough northwest of Pakistan rather than the structure and evolution of the jet itself.

An important contributor to the flooding rains over Pakistan on 27–30 July was the advection of deep tropical monsoonal moisture from Bangladesh and the Bay of Bengal to northern Pakistan, in agreement with Houze et al. (2011), Lau and Kim (2012), and Webster et al. (2011). As also shown by Houze et al. (2011), anticyclogenesis over the Tibetan Plateau during the latter part of July generated tropospheric-deep anomalous easterly flow over northern India, which is rare in heavy rainfall events over northern Pakistan and northwest India as shown by Romatschke and Houze (2011). Our results additionally show that the Tibetan anticyclone was a key feature that was absent during the previous rain events over northern Pakistan in June and July 2010, and was a key factor that increased the relative severity of the 27–30 July event. Our analysis also revealed that a westward-moving monsoon depression drove an intense low-level southeasterly jet along the equatorward flank of the Tibetan anticyclone, complementing the findings in Houze et al. (2011). The results also suggest that the monsoon depression formed in conjunction with a broad region of enhanced convection related to the MJO, and that the low-level southeasterly jet had characteristics of a barrier jet. The implication of the barrier jet is that it produced a region of intense upslope flow during 28–29 July, which helped anchor the region of widespread convection to the elevated orography in a synoptic environment already favorable for heavy rainfall. Building on findings in Houze et al. (2011), our results show that the intense barrier jet–like feature, and robust upslope flow, were key factors that were absent for previous rain events, again likely contributing to the relative increased severity of the 27–30 July rain event. A possible avenue of future work would be to use a high-resolution numerical simulation to examine the mechanisms for barrier jet formation (e.g., via a momentum budget), and more definitively show that the low-level jet was a true barrier jet. The sparse

observations and relatively coarse resolution of the global analysis grids are not able to fully resolve the processes that may drive barrier jet formation.

Acknowledgments. This study is supported by (i) NOAA's THORPEX program and (ii) a CIRES visiting fellowship. Conversations with Rich Grumm (NOAA/NWS) and Prof. Russ Schumacher (Colorado State University), and feedback received during a scientific map discussion at the Physical Sciences Division in the NOAA/Earth System Research Laboratory led by the lead author, contributed to this work. Dave Vollaro (University at Albany, SUNY) is thanked for help in processing the TRMM rainfall data. Dr. Klaus Wolter (CIRES/University of Colorado) is thanked for collecting and tabulating climatological rainfall information over Pakistan. Prof. Lance Bosart (University at Albany, SUNY) is thanked for providing an informal review on an earlier version of the manuscript. Three anonymous reviewers are thanked for their critical comments and suggestions.

REFERENCES

Barriopedro, D., E. M. Fischer, J. Luterbacher, R. M. Trigo, and R. Garcia-Herrera, 2011: The hot summer of 2010: Redrawing the temperature record map of Europe. *Science,* **332,** 220–224.

Bell, G. D., and L. F. Bosart, 1988: Appalachian cold-air damming. *Mon. Wea. Rev.,* **116,** 137–161.

Black, E., M. Blackburn, G. Harrison, B. Hoskins, and J. Methven, 2004: Factors contributing to the summer 2003 European heatwave. *Weather,* **59,** 217–223.

Buizza, R., C. Cardinali, G. Kelly, and J.-N. Thépaut, 2007: The value of observations. Part II: The value of observations located in singular-vector-based target areas. *Quart. J. Roy. Meteor. Soc.,* **133,** 1833–1842.

Burt, S., 2004: The August 2003 heatwave in the United Kingdom. Part I: Maximum temperatures and historical precedents. *Weather,* **59,** 199–208.

Caracena, F., R. A. Maddox, L. R. Hoxit, and C. F. Chappell, 1979: Mesoanalysis of the Big Thompson storm. *Mon. Wea. Rev.,* **107,** 1–17.

Changnon, S. A., K. E. Kunkel, and B. C. Reinke, 1996: Impacts and responses to the 1995 heat wave: A call to action. *Bull. Amer. Meteor. Soc.,* **77,** 1497–1506.

Chen, W.-D., and R. B. Smith, 1987: Blocking and deflection of airflow by the Alps. *Mon. Wea. Rev.,* **115,** 2578–2597.

Dole, R., and Coauthors, 2011: Was there a basis for anticipating the 2010 Russian heat wave? *Geophys. Res. Lett.,* **38,** L06702, doi:10.1029/2010GL046582.

Galarneau, T. J., Jr., and L. F. Bosart, 2006: Ridge rollers: Mesoscale disturbances on the periphery of cutoff anticyclones. Preprints, *Severe Local Storms Special Symp.,* Atlanta, GA, Amer. Meteor. Soc., P1.11. [Available online at http://ams.confex.com/ams/pdfpapers/103464.pdf.]

——, ——, and A. R. Aiyyer, 2008: Closed anticyclones of the subtropics and midlatitudes: A 54-yr climatology (1950–2003) and three case studies. *Synoptic–Dynamic Meteorology and Weather Analysis and Forecasting: A Tribute to Fred Sanders, Meteor. Monogr.,* No. 55, Amer. Meteor. Soc., 349–392.

Ghelli, A., A. Garcia-Mendez, F. Prates, and M. Dahoui, 2010: Extreme weather events in summer 2010: How did the ECMWF forecasting systems perform? *ECMWF Newsletter,* No. 125, ECMWF, Reading, United Kingdom, 7–11.

Grumm, R. H., 2011: The central European and Russian heat event of July–August 2010. *Bull. Amer. Meteor. Soc.,* **92,** 1285–1296.

Hakim, G. J., and R. D. Torn, 2008: Ensemble synoptic analysis. *Synoptic–Dynamic Meteorology and Weather Analysis and Forecasting: A Tribute to Fred Sanders, Meteor. Monogr.,* No. 55, Amer. Meteor. Soc., 147–161.

Hao, W., and L. F. Bosart, 1987: A moisture budget analysis of the protracted heat wave in the southern Plains during the summer of 1980. *Wea. Forecasting,* **2,** 269–288.

Hong, C.-C., H.-H. Hsu, N.-H. Lin, and H. Chiu, 2011: Roles of European blocking and tropical-extratropical interaction in the 2010 Pakistan flooding. *Geophys. Res. Lett.,* **38,** L13806, doi:10.1029/2011GL047583.

Hoskins, B. J., M. E. McIntyre, and A. W. Robertson, 1985: On the use and significance of isentropic potential vorticity maps. *Quart. J. Roy. Meteor. Soc.,* **111,** 877–946.

Houze, R. A., Jr., D. C. Wilton, and B. F. Smull, 2007: Monsoon convection in the Himalayan region as seen by the TRMM Precipitation Radar. *Quart. J. Roy. Meteor. Soc.,* **133,** 1389–1411.

——, K. L. Rasmussen, S. Medina, S. R. Brodzik, and U. Romatschke, 2011: Anomalous atmospheric events leading to the summer 2010 floods in Pakistan. *Bull. Amer. Meteor. Soc.,* **92,** 291–298.

Hoyos, C. D., and P. J. Webster, 2007: The role of intraseasonal variability in the nature of Asian monsoon precipitation. *J. Climate,* **20,** 4402–4424.

Huffman, G. J., R. F. Adler, S. Curtis, D. T. Bolvin, and E. J. Nelkin, 2007: Global rainfall analyses at monthly and 3-hr time scales. *Measuring Precipitation from Space: EURAINSAT and the Future,* V. Levizzani, P. Bauer, and F. Joseph Turk, Eds., Springer, 291–306.

Johns, R. H., and W. D. Hirt, 1987: Derechos: Widespread convectively induced windstorms. *Wea. Forecasting,* **2,** 32–49.

Kalnay, E., and Coauthors, 1996: The NCEP/NCAR 40-Year Reanalysis Project. *Bull. Amer. Meteor. Soc.,* **77,** 437–471.

Kleist, D. T., K. Ide, J. Whitaker, J. C. Derber, D. Parrish, and X. Wang, 2011: Expanding the GSI-based hybrid ensemble-variational system to include more flexible parameter settings. Preprints, *15th Symp. on Integrated Observing and Assimilation Systems for the Atmosphere, Oceans and Land Surface (IOAS-AOLS),* Seattle, WA, Amer. Meteor. Soc. [Available online at http://ams.confex.com/ams/91Annual/webprogram/Paper180096.html.]

Kumar, K. K., B. Rajagopatan, M. Hoerling, G. Bates, and M. Cane, 2006: Unraveling the mystery of Indian monsoon failure during El Niño. *Science,* **314,** 115–119.

Lau, W. K. M., and K.-M. Kim, 2012: The 2010 Pakistan flood and Russian heat wave: Teleconnection of hydrometeorological extremes. *J. Hydrometeor.,* **13,** 392–403.

Lawrence, D. M., and P. J. Webster, 2001: Interannual variations of the intraseasonal oscillation in the South Asian summer monsoon region. *J. Climate,* **14,** 2910–2922.

Li, J., and Y.-L. Chen, 1998: Barrier jets during TAMEX. *Mon. Wea. Rev.,* **126,** 959–971.

Lin, Y.-L., S. Chiao, T.-A. Wang, M. L. Kaplan, and R. P. Weglarz, 2001: Some common ingredients for heavy orographic rainfall. *Wea. Forecasting,* **16,** 633–660.

Livezey, R. E., and R. Tinker, 1996: Some meteorological, climatological, and microclimatological considerations of the severe U.S. heat wave of mid-July 1995. *Bull. Amer. Meteor. Soc.,* **77,** 2043–2054.

Lyon, B., and R. M. Dole, 1995: A diagnostic comparison of the 1980 and 1988 U.S. summer heat wave–droughts. *J. Climate,* **8,** 1658–1675.

Madden, R., and P. Julian, 1972: Description of global-scale circulation cells in the tropics with a 40–50 day period. *J. Atmos. Sci.,* **29,** 1109–1123.

Maddox, R. A., L. R. Hoxit, C. F. Chappell, and F. Caracena, 1978: Comparison of meteorological aspects of the Big Thompson and Rapid City flash floods. *Mon. Wea. Rev.,* **106,** 375–389.

Massacand, A. C., H. Wernli, and H. C. Davies, 1998: Heavy precipitation on the Alpine southside: An upper-level precursor. *Geophys. Res. Lett.,* **25,** 1435–1438.

Matsueda, M., 2011: Predictability of Euro-Russian blocking in summer of 2010. *Geophys. Res. Lett.,* **38,** L06801, doi:10.1029/2010GL046557.

Mo, K. C., J. Nogues-Paegle, and J. Paegle, 1995: Physical mechanisms of the 1993 summer floods. *J. Atmos. Sci.,* **52,** 879–895.

Namias, J., 1936: Structure and maintenance of dry-type moisture discontinuities not developed by subsidence. *Mon. Wea. Rev.,* **64,** 351–358.

——, 1982: Anatomy of Great Plains protracted heat waves (especially the 1980 U.S. summer drought). *Mon. Wea. Rev.,* **110,** 824–838.

——, 1991: Spring and summer 1988 drought over the contiguous United States—Causes and prediction. *J. Climate,* **4,** 54–65.

Olson, J. B., B. A. Colle, N. A. Bond, and N. Winstead, 2007: A comparison of two coastal barrier jet events along the southeast Alaskan coast during the SARJET field experiment. *Mon. Wea. Rev.,* **135,** 2973–2994.

Pan, Z., M. Segal, and R. W. Aritt, 2004: Role of topography in forcing low-level jets in the central United States during the 1993 flood-altered terrain simulations. *Mon. Wea. Rev.,* **132,** 396–403.

Pelly, J. L., and B. J. Hoskins, 2003: A new perspective on blocking. *J. Atmos. Sci.,* **60,** 743–755.

Plumb, R. A., 1985: On the three-dimensional propagation of stationary waves. *J. Atmos. Sci.,* **42,** 217–229.

Pontrelli, M. D., G. Bryan, and J. M. Fritsch, 1999: The Madison County, Virginia, flash flood of 27 June 1995. *Wea. Forecasting,* **14,** 384–404.

Rodwell, M. J., and B. J. Hoskins, 1996: Monsoons and the dynamics of deserts. *Quart. J. Roy. Meteor. Soc.,* **122,** 1385–1404.

Romatschke, U., and R. A. Houze Jr., 2011: Characteristics of precipitating convective systems in the premonsoon season of South Asia. *J. Hydrometeor.,* **12,** 157–180.

——, S. Medina, and R. A. Houze Jr., 2010: Regional, seasonal, and diurnal variations on convection in the South Asian monsoon region. *J. Climate,* **23,** 419–439.

Rotunno, R., and R. Ferretti, 2001: Mechanisms of intense Alpine rainfall. *J. Atmos. Sci.,* **58,** 1732–1749.

Schutts, G. J., 1983: The propagation of eddies in effluent jet streams: Eddy vorticity forcing of 'blocking' flow fields. *Quart. J. Roy. Meteor. Soc.,* **109,** 737–761.

Shukla, J., and D. A. Paolina, 1983: The southern oscillation and long range forecasting of the summer monsoon rainfall over India. *Mon. Wea. Rev.,* **111,** 1830–1837.

Srock, A. F., and L. F. Bosart, 2009: Heavy precipitation associated with southern Appalachian cold-air damming and Carolina coastal frontogenesis in advance of weak landfalling Tropical Storm Marco (1990). *Mon. Wea. Rev.,* **137,** 2448–2470.

Weaver, S. C., and S. Nigam, 2008: Variability of the Great Plains low-level jet: Large-scale circulation context and hydroclimate impacts. *J. Climate,* **21,** 1532–1551.

Webster, P. J., and C. D. Hoyos, 2004: Prediction of monsoon rainfall and river discharge on 15–30-day time scales. *Bull. Amer. Meteor. Soc.,* **85,** 1745–1765.

——, V. E. Toma, and H.-M. Kim, 2011: Were the 2010 Pakistan floods predictable? *Geophys. Res. Lett.,* **38,** L04806, doi:10.1029/2010GL046346.

Wheeler, M. C., and H. H. Hendon, 2004: An all-season real-time multivariate MJO index: Development of an index for monitoring and prediction. *Mon. Wea. Rev.,* **132,** 1917–1932.

Zipser, E. J., D. J. Cecil, C. Liu, S. W. Nesbitt, and D. P. Yorty, 2006: Where are the most intense thunderstorms on Earth? *Bull. Amer. Meteor. Soc.,* **87,** 1057–1071.